

Development and verification of a coupled DSMC–NS scheme using unstructured mesh

J.-S. Wu^{a,*}, Y.-Y. Lian^a, G. Cheng^b, R.P. Koomullil^b, K.-C. Tseng^a

^a Department of Mechanical Engineering, National Chiao-Tung University, 1001 Ta-Hsueh Road, Hsinchu 30050, Taiwan

^b Department of Mechanical Engineering, University of Alabama at Birmingham, AL 35294-4461, USA

Received 23 April 2005; received in revised form 22 February 2006; accepted 4 April 2006

Available online 14 June 2006

Abstract

An efficient and accurate parallel coupled DSMC–NS method using three-dimensional unstructured grid topology is proposed and verified for the simulation of high-speed gas flows involving continuum and rarefied regimes. A domain overlapping strategy, taking advantage of unstructured data format, with Dirichlet–Dirichlet type boundary conditions based on two breakdown parameters is used iteratively to determine the choice of solvers in the spatial domain. The selected breakdown parameters for this study include: (1) a local maximum Knudsen number defined as the ratio of the local mean free path and local characteristic length based on property gradient and (2) a thermal non-equilibrium indicator defined as the ratio of the difference between translational and rotational temperatures to the translational temperature. A supersonic flow ($M_\infty = 4$) over a quasi-2-D 25° wedge is employed as the first step in verifying the present coupled method. The results of simulation using the coupled method are in excellent agreement with those of the pure DSMC method, which is taken as the benchmark solution. Effects of the size of overlapping regions and the choice of breakdown parameters on the convergence history are discussed. Results show that the proposed iteratively coupled method predicts the results more accurately as compared to the “one-shot” coupled method, which has been often used in practice. Further, a realistic 3-D nitrogen flow, which two near-continuum parallel orifice jets underexpand into a near-vacuum environment, is simulated using the present coupled method to demonstrate its capability. Finally, developments in extending the present method are also outlined in this paper.

© 2006 Elsevier Inc. All rights reserved.

Keywords: Direct simulation Monte Carlo; Coupled method; Rarefied gas flow; Navier–Stokes solver; Supersonic flows

1. Introduction

Hypersonic flows of practical importance often involve flow fields having continuum and rarefied regions, e.g. blunt body wakes, sharp leading edges, and expanding reaction control system plumes [1,2]. It is well known the direct simulation Monte Carlo (DSMC) method [3] can provide more physically accurate results

* Corresponding author. Tel.: +886 3 573 1693; fax: +886 3 572 0634.

E-mail address: chongsin@faculty.nctu.edu.tw (J.-S. Wu).

in flows having rarefied and non-equilibrium regions than continuum flow models. However, the DSMC method is extremely computational expensive especially in the near-continuum region, which prohibits its applications to practical problems with complex geometries and large domains. In contrast, the computational fluid dynamics (CFD) method, employed to solve the Navier–Stokes (NS) or Euler equation for continuum flows, is computationally efficient in simulating a wide variety of flow problems. But the use of continuum theories for the flow problems involving the rarefied gas or very small length scales (equivalently large Knudsen numbers) can produce inaccurate results due to the breakdown of continuum assumption or thermal equilibrium. A practical approach for solving the flow fields having near-continuum to rarefied gas is to develop a numerical model combining the CFD method for the continuum regime with the DSMC method for the rarefied and thermal non-equilibrium regime. A well-designed hybrid scheme is expected to take advantage of both the computational efficiency and accuracy of the NS solver in the continuum regime and the physical accuracy of the DSMC method in the rarefied or thermal non-equilibrium regime. Past efforts in developing such a hybrid method are reviewed and summarized below.

Aktas and Aluru [4] proposed a multi-scale method that combines the Stokes equation solver with the DSMC method, which was used for the analysis of micro-fluidic filters. The continuum regions were governed by Stokes equations solved by a scattered point finite cloud method. The continuum and DSMC regions were coupled through an overlapped Schwarz alternating method with Dirichlet–Dirichlet type boundary conditions. However, the interface location between two solvers was specified in advance. Garcia et al. [5] constructed a hybrid particle/continuum algorithm with an adaptive mesh and algorithm refinement, which was designed to treat multi-scale flow problems. The DSMC method was used as a particle method embedded within a Godunov-type compressible Navier–Stokes solver. This methodology is especially useful when local mesh refinement for the continuum solver becomes inappropriate as the grid size approaches the molecular scales. Glass and Gnoffo [6] proposed “one-shot” coupled 3-D CFD–DSMC method for the simulation of highly blunt bodies using the structured grid under steady-state conditions. Interfacial location between the CFD and DSMC zones was identified manually after one-shot CFD simulation. Results of CFD simulation at this interface were then used as the inflow boundary conditions (Dirichlet type) for the DSMC method in the rarefied regions. Wang et al. [7] proposed a hybrid information preservation/Navier–Stokes (IP-NS) method to reduce statistical uncertainties during the process of coupling. This method is potentially suitable for simulating unsteady flows. Roveda et al. [8] also proposed a hybrid Euler–DSMC approach for unsteady flow simulations. Two special approaches were designed to reduce statistical uncertainties at the interface during the coupling procedures: (1) use of an overlapped region between the DSMC and Euler zones and (2) use of a “ghost level structure” to reduce statistical uncertainties. However, cloning of particles is required in this approach and may be problematic in a particle method such as DSMC. At present, only one-dimensional and two-dimensional flows were demonstrated in the literature and extension to parallel or three-dimensional simulation has not been reported to the best knowledge of the authors.

In general, a hybrid DSMC–NS method applies the concept of spatial domain decomposition to distinguish the computational domain of rarefaction or thermal non-equilibrium to be modeled by the DSMC method, and the computational domain of continuum to be solved by the CFD (NS, Euler or Stokes) solver. Success of such hybrid numerical method relies upon three important factors: (1) Correctness in identifying the location of spatial interface between the DSMC and continuum method during computation. Proper location of the interface not only guarantees a physically correct simulation, but also helps to possibly optimize (or reduce) the computational time. It is expected to design some criteria that can be used to efficiently and accurately identify the interface and be easily evaluated during runtime. (2) Properly and efficiently exchanging interfacial information (or flow properties) during runtime. In practice, one side of the interface is the DSMC method with accuracy strongly depending upon the sampling statistics. The computational efficiency and accuracy of the continuum solver can be potentially jeopardized by the possibly noisy boundary conditions if the uncertainty of statistical sampling is large. (3) The effect of steadiness of the flow solution on designing data exchange at the interface. In the case of unsteady simulations, the algorithm for data exchange can be very complicated in order to keep the statistical uncertainties of the particle method as low as possible.

In the current study, a parallel coupled DSMC–NS method using three-dimensional unstructured mesh, capable of efficiently and correctly simulating steady flows, consisting of both continuum and rarefied regions is proposed and verified. Steady-state simulations were performed to reduce the complexity in the coupling

process and to verify the present coupled DSMC–NS method. Possible issues related to the extension of the present approach to unsteady flows are addressed at the end of the paper.

The present paper is organized as follows. The proposed coupled DSMC–NS method is described in detail in Section 2 followed by the results and discussions based on the simulation of a supersonic nitrogen flow past a quasi-2-D wedge flow. Further, a realistic 3-D nitrogen flow, which two near-continuum parallel orifice jets underexpand into a near-vacuum environment, is simulated using the present coupled method to demonstrate its superior capability. Finally, the conclusions of the current study are summarized with possible future developments and enhancements.

2. Coupled DSMC–NS method

In the proposed coupled DSMC–NS method, steady-state flow calculation is assumed. There are two numerical flow solvers included: one is the 3-D DSMC code for rarefied and thermally non-equilibrium regions, named PDSC (parallel direct simulation Monte Carlo code), developed by Wu's group [9–12] and the other is HYB3D, a 3-D Euler and Navier–Stokes solver for continuum regions, developed by Koomullil [13–16]. It is rather straightforward to exchange the information between the PDSC and HYB3D in the present coupled DSMC–NS method because both methods use the unstructured grid topology with parallel computing. However, coupling procedures proposed in the current study are not limited to any specific codes, and selection of these two solvers is for the purpose of demonstration. Both codes are introduced briefly in the following, respectively, for completeness.

2.1. DSMC solver (PDSC)

Important features of the PDSC code can be found in the Refs. [9–12] and are briefly described in the following.

- (1) *3-D unstructured-grid topology*: PDSC can accept either tetrahedral, hexahedral or hybrid tetrahedral–hexahedral mesh [12]. Computational cost of particle tracking for the unstructured mesh is generally higher than that for the structured mesh. However, the use of the unstructured mesh, which provides excellent flexibility of handling boundary conditions with complicated geometry and of parallel computing using dynamic domain decomposition based on load balancing, is highly justified.
- (2) *Parallel computing using dynamic domain decomposition*: Load balancing of PDSC is achieved by repeatedly repartitioning the computational domain using a multi-level graph-partitioning tool, PMETIS [17,18], by taking advantage of the unstructured mesh topology employed in the code. A decision policy for repartition with a concept of Stop-At-Rise (SAR) [19] or constant period of time (fixed number of time steps) can be used to decide when to repartition the domain. Capability of repartitioning of the domain at constant or variable time interval is also provided in PDSC. Resulting parallel performance is excellent if the problem size is comparably large. Details can be found in Wu and Tseng [9].
- (3) *Variable time-step scheme*: PDSC employs a variable time-step scheme (or equivalently a variable cell-weighting scheme), based on particle flux (mass, momentum, energy) conservation when particles pass interface between cells. This strategy can greatly reduce both the number of iterations towards the steady-state, and the required number of simulated particles for an acceptable statistical uncertainty. Past experience shows this scheme is very effective when coupled with an adaptive mesh refinement technique [11].

In the current coupled DSMC–NS method, PDSC only computes those regions, including continuum breakdown, thermal non-equilibrium and overlapping. Before DSMC computation at each coupling iteration, the new numbering of the DSMC cells is created based on the new DSMC domain(s) for saving memory cost in DSMC simulation. This is done due to: (1) The DSMC solver is more memory expensive than the NS solver with the same mesh size. (2) Only part of the mesh used in the initial NS simulation is required in the DSMC simulation.

2.2. Navier–Stokes solver (HYB3D)

The HYB3D is a Navier–Stokes solver using a generalized- or an unstructured-grid topology and has the following important features: (1) cell-centered finite-volume upwind scheme for the numerical integration of governing equations, (2) Roe’s approximate Riemann solver for convective flux evaluation, (3) parallel computing using message passing interface (MPI), (4) laminar or turbulent flow simulation capability with various turbulence models, and (5) application of overset grid topology for flow simulation over moving or complex bodies. Implicit time integration is used with local time stepping, where the maximum allowable time step in each cell is determined by the CFL condition constrained by advection and viscous stability criteria. A second order spatial accuracy is achieved using Taylor’s series expansion and the gradients of the flow properties are computed using a least-square method. The creation of local extreme during the higher order linear reconstruction is eliminated by the application of Venkatakrisnan’s type [20] limiter. Parallel computing of the HYB3D also incorporates the graph-partition tool, METIS, which is the same as that in the PDSC. The dynamic domain decomposition in the current HYB3D computation is circumvented by not adaptively refining in this phase of computation. Note the HYB3D, unlike some other multiple-temperature NS codes, is developed with thermal equilibrium assumption. Thus, thermal non-equilibrium becomes an important issue while defining the appropriate NS domain(s) in the present coupled method.

Extensive validation of the numerical algorithms that are used in the Navier–Stokes simulation code has been conducted earlier and has been reported in the literature [16,23,24]. Also, the effects of the two different limiters by Barth and Jespersen [25], and Venkatakrisnan [26] for the generalized grid based Navier–Stokes solver have been studied and have been reported in Koomullil [23]. In addition, as can be seen later, shock regions are generally computed by the DSMC code during the iterative process, which renders the selection of limiter unimportant.

2.2.1. Breakdown parameters

The first issue in developing the coupled DSMC–NS method is how to determine both the appropriate computational domain for the DSMC and NS solvers, and the proper interface boundary between these two solvers. A continuum breakdown parameter, proposed by Wang and Boyd [21] for hypersonic flows, is employed in the present coupled DSMC–NS method as one of the criteria for selecting proper solvers. The continuum breakdown parameter Kn_{\max} is defined as

$$Kn_{\max} = \max[Kn_D, Kn_V, Kn_T] \quad (1)$$

where Kn_D , Kn_V and Kn_T are the local Knudsen numbers based on density, velocity and temperature, respectively. They can be calculated from the following general formula:

$$Kn_Q = \frac{\lambda}{Q} |\nabla Q| \quad (2)$$

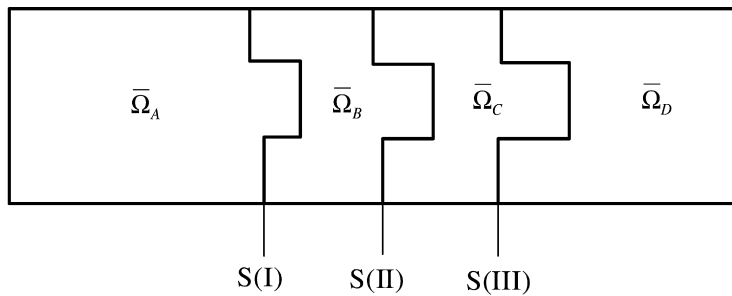
where Q is the specific flow property (density, velocity and temperature) and λ is the local mean free path. If the calculated value of the continuum breakdown parameter in a region is larger than a preset threshold value Kn_{\max}^{Thr} , then it cannot be modeled using the NS equation. Instead, a particle solver like DSMC has to be used for that region.

In addition, another breakdown parameter is used to identify regions that exhibit thermal non-equilibrium among various degrees of freedom. This parameter can correctly define the region of thermal-equilibrium breakdown as a thermal-equilibrium NS solver like the HYB3D code is chosen in the coupled method. The breakdown parameter of thermal equilibrium is proposed to be the ratio of the difference between translational and rotational temperatures to translational temperature in the present study, if diatomic gas molecules at moderate temperature are involved in the simulation. Indeed, the definition of this parameter for atomic gas can be easily extended to the ratio of the difference between two translational temperatures to any specific translational temperature. For high-temperature flows, vibrational degrees of freedom may be also used to define this thermal non-equilibrium indicator. In the current study, this thermal non-equilibrium indicator is defined as

$$P_{Tne} = \left| \frac{T_{Tr} - T_R}{T_{Tr}} \right| \tag{3}$$

where T_{Tr} and T_R are translational and rotational temperature, respectively. If the value of the computed thermal non-equilibrium indicator in a region is larger than some preset threshold value P_{Tne}^{Thr} in the current study, then this flow region cannot be modeled correctly by those NS equation solvers, such as the currently used HYB3D code, which assumes thermal equilibrium among various degrees of freedom. Hence, the DSMC method has to be used for that region instead. Note the parameter P_{Tne} defined in Eq. (3) can be calculated only by DSMC, because HYB3D does not have the multi-temperature modeling capability. This means it can only serve simultaneously with the Knudsen numbers (Eq. (1)) to control a potential switch back from DSMC to NS for those regions where the thermal non-equilibrium effect disappears after iterating between DSMC and NS methods.

Some comments address the use of the single-temperature Maxwellian distribution function at the interface of DSMC and NS regions in the proposed coupled method as follows. Use of multiple-temperature NS equation solver could help to model the thermal non-equilibrium in much extended (into DSMC region) NS region; however, two or more energy (or temperature) equations have to be solved in all NS regions. In addition,



$$\bar{\Omega}_A : \left\{ \bar{\Omega}_{P_{Tne}} \cup \bar{\Omega}_{Kn_{max}} \right\} \text{ Union of continuum breakdown and thermal non-equilibrium regions}$$

$\bar{\Omega}_B$: The extension of $\bar{\Omega}_A$ with some specified number of cell layers

$\bar{\Omega}_C$: The further extension of $\bar{\Omega}_B$ with some specified number of cell layers

$\bar{\Omega}_A \cup \bar{\Omega}_B \cup \bar{\Omega}_C$: DSMC simulation domain

$\bar{\Omega}_B \cup \bar{\Omega}_C \cup \bar{\Omega}_D$: NS solver simulation domain

$\bar{\Omega}_A \cup \bar{\Omega}_B$: Domain with flow properties updated from DSMC calculation

$\bar{\Omega}_C \cup \bar{\Omega}_D$: Domain with flow properties updated from NS calculation

$S(I) = \bar{\Omega}_A \cap \bar{\Omega}_B$: Boundary-I (Dirichlet B.C.) for NS simulations

$S(II) = \bar{\Omega}_B \cap \bar{\Omega}_C$: Boundary-II for updated solution using different solvers

$S(III) = \bar{\Omega}_C \cap \bar{\Omega}_D$: Boundary-III (Dirichlet B.C.) for DSMC simulations

Fig. 1. Sketch of numerical domain distribution of the present coupled DSMC–NS method with overlapping regions and boundaries.

extended NS region into DSMC region (larger property gradients or more rarefied) may further deteriorate the inherent assumption of Maxwellian distribution function in each degree of freedom in the multiple-temperature NS equation solver. Thus, use of two- or multiple-temperature NS solver may possibly benefit in reducing computational efforts, while it may introduce inaccuracy from physical point of view.

Furthermore, Chapman–Enskog distribution temperature and density gradients may have to be used at the interface of DSMC and NS regions where slight thermal non-equilibrium is considered. Its use would, however, greatly increase the computational cost as demonstrated in Garcia and Alder [27] since more random number calls and computational operations are required. In practice, use of the single-temperature Maxwellian distribution function at the interface of DSMC and NS regions is much easier and with less computational cost. By taking the above intertwining factors into account, proposed coupled DSMC–NS scheme simply utilizes Maxwellian distribution function at the DSMC–NS interface by properly controlling the magnitude of the breakdown parameters and the appropriate overlapping regions that extends the DSMC region.

Based on the breakdown parameters, calculated from the preliminary simulation data using the continuum flow solver (HYB3D), and the criteria for the breakdowns of the continuum theory and thermal equilibrium, the domain for suitable DSMC simulation can be determined properly. Detailed procedures of determining the boundary (Boundary-I) between the DSMC and NS approaches and marking the breakdown domain $\bar{\Omega}_A$ are shown in Algorithm 1.

In Algorithm 1, distribution of breakdown parameters and the array of right-hand and left-hand cells for each cell interface are first read in. In Algorithm 1, the right-hand cell is indexed as “iR”, while the left-hand cell is indexed as “iL”, as both shown schematically in Algorithm 1. This face-based array, which is built up using the element connectivity before the simulation, represents the numbering of two cells that share the common cell face. All cells and cell faces are then initialized, respectively, to be neither a continuum breakdown region ($\bar{\Omega}_A$) nor a Boundary-I face. Note that the notations used in the current study can be found in Fig. 1 with explanation that will be introduced shortly. All cells and cell faces are then checked, respectively, to decide if they are part of $\bar{\Omega}_A$ and interface Boundary-I. Using this subroutine, breakdown ($\bar{\Omega}_A$) and non-breakdown regions ($\bar{\Omega}_B \cup \bar{\Omega}_C \cup \bar{\Omega}_D$), and Boundary-I can be properly identified for the entire computational domain.

2.2.2. Overlapping regions between DSMC and NS domain

Fig. 1 shows the sketch of overlapping regions and boundaries near the interface of the DSMC and NS solvers at an intermediate step (other than the first CFD simulation step for the whole domain). Related symbols and notation are listed and explained below the sketch in Fig. 1. The general iterative procedure of the

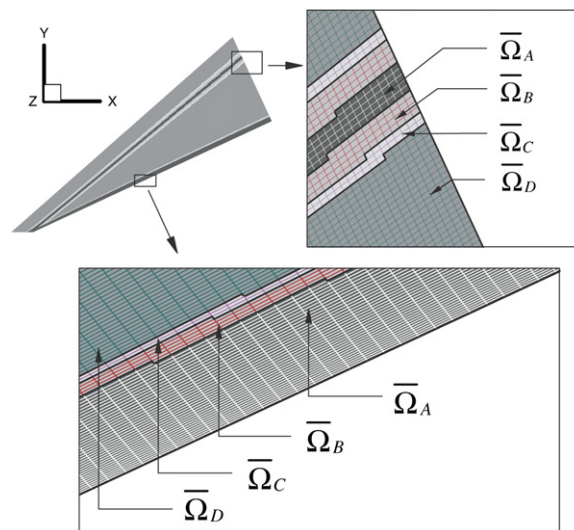


Fig. 2. A typical example of the overlapping regions between the particle and the continuum domains.

present coupling framework is that running the DSMC solver first after the breakdown regions are identified, and then running the NS solver next with the boundary values calculated from DSMC simulations. We now focus on the overlapping regions and boundaries in Fig. 1, which is important in understanding the coupling procedures. Note that all domains mentioned in the following include the boundaries surrounding them. Domain $\overline{\Omega}_A \cup \overline{\Omega}_B \cup \overline{\Omega}_C$ represents the DSMC simulation region, while domain $\overline{\Omega}_B \cup \overline{\Omega}_C \cup \overline{\Omega}_D$ represents the NS simulation region; thus, domain $\overline{\Omega}_B \cup \overline{\Omega}_C$ is the designated overlapping region. Boundary conditions (Dirichlet-type) on Boundary-I ($= \overline{\Omega}_A \cap \overline{\Omega}_B$) for NS simulation come from part of the previous iterative DSMC simulation, while boundary conditions (Dirichlet-type) on Boundary-III ($= \overline{\Omega}_C \cap \overline{\Omega}_D$) for DSMC simulation come from part of the previous iterative NS solution. Location of Boundary-I is determined from strict comparison of breakdown parameters (Kn_{\max} and P_{Tne}), computed based on previous iterative solution of domain $\overline{\Omega}_A \cup \overline{\Omega}_B \cup \overline{\Omega}_C \cup \overline{\Omega}_D$, with the preset criteria. Location of Boundaries-II and -III are then determined by extending from Boundary-I towards the neighboring continuum region. In addition, the “thickness” (number of cell layers) of domains $\overline{\Omega}_B$ and $\overline{\Omega}_C$ can be adjusted to achieve better convergence for the coupling procedure.

A typical example of the overlapping regions in practice is demonstrated in Fig. 2. It shows $\overline{\Omega}_B$ is the extension of $\overline{\Omega}_A$ towards its neighboring continuum regions with 4 cell layers, while $\overline{\Omega}_C$ is its further extension in the same direction with 2 cell layers. Size of overlapping regions can be adjusted depending upon the numbers of cell layers for $\overline{\Omega}_B$ and $\overline{\Omega}_C$, respectively. Overlapping regions and boundaries of the DSMC domain is in general slightly larger than which is strictly determined based on the distribution of breakdown parameters. This is justified in physics because DSMC can intrinsically simulate all regimes of gas flows if computational cost is not a concern. In addition, the method of introducing particles from the interface boundaries into the DSMC domain can be further simplified by only using Maxwellian velocity distribution since the flow is very close to equilibrium condition. An algorithm for generating overlapping regions and locating Boundary-III is also shown in Algorithm 2, which is explained briefly as follows.

In Algorithm 2, only overlapping regions ($\overline{\Omega}_B$, $\overline{\Omega}_C$, and $\overline{\Omega}_D$) and Boundary-III are identified, while Boundary-II is not identified specifically. The reason is that only Boundary-I and Boundary-III are the locations which require imposing boundary conditions for NS and DSMC solvers, respectively, while Boundary-II only serves as the interface for updating solutions. Details of Algorithm 2 are skipped since it is rather self-explanatory. The main idea of this algorithm is to keep track of the list of current interface nodes originating from Boundary-I interface and to extend the necessary number of cell layers in the direction of non-breakdown regions ($\overline{\Omega}_B \cup \overline{\Omega}_C \cup \overline{\Omega}_D$). Also, the number of cell layers of $\overline{\Omega}_B$ and $\overline{\Omega}_C$ can be adjusted in this subroutine (Algorithm 2), respectively.

Furthermore, in the current coupled DSMC–NS method the choice of solution update for each cell is based on its domain type. Domain $\overline{\Omega}_A \cup \overline{\Omega}_B$ is the region where the updated solution comes from the DSMC simulation, while domain $\overline{\Omega}_C \cup \overline{\Omega}_D$ is the region where the updated solution comes from the NS simulation.

2.2.3. Coupling procedures

The second issue of the coupled method is the information exchange through the interface between the NS domain and the DSMC domain. Algorithm 3 summarizes general procedures of current coupled DSMC–NS method, which will be explained in detail shortly. In addition, Algorithm 4 describes the procedures about how the macroscopic flow properties at the Boundary-III, calculated from the previous NS simulation, are used as the new Dirichlet-type boundary conditions and fed into the DSMC solver for domain $\overline{\Omega}_A \cup \overline{\Omega}_B \cup \overline{\Omega}_C$. Flow properties on both sides of Boundary-III, calculated from NS simulation, are averaged as the boundary conditions for the DSMC solver. From the DSMC simulation, the macroscopic flow properties at Boundary-I are employed as the Dirichlet-type boundary conditions and fed back to the NS solver for domain $\overline{\Omega}_B \cup \overline{\Omega}_C \cup \overline{\Omega}_D$. Detailed procedures of extracting data on Boundary-I are presented in Algorithm 5, which is similar to Algorithm 4. Since steady flow is assumed, coupling between the DSMC and NS solvers at each integration time step is not necessary. Statistical uncertainty from the DSMC simulation can thus be minimized if enough sampling at each iteration step is accumulated. Generally, less than 10 couplings are good enough to achieve converged solution, which will be shown in Section 3.

In brief summary, major procedures of the present coupled DSMC–NS method are listed as follows (Algorithm 3):

1. Apply the HYB3D code to simulate the whole flow field as continuum.
2. Determine the locations of Boundary-I and -III and, thus, the DSMC simulation domain ($\overline{\Omega}_A \cup \overline{\Omega}_B \cup \overline{\Omega}_C$).
3. Impose Dirichlet-type boundary conditions (velocities, temperature and number density) on Boundary-III, obtained from latest NS simulation, for the next DSMC simulation domain ($\overline{\Omega}_A \cup \overline{\Omega}_B \cup \overline{\Omega}_C$).
4. Simulate and sample the flow field in the DSMC domain ($\overline{\Omega}_A \cup \overline{\Omega}_B \cup \overline{\Omega}_C$), using the PDSC code, until acceptable statistical uncertainties are reached.
5. Impose Dirichlet-type boundary conditions (velocities, temperature and density) on Boundary-I, obtained from latest DSMC simulation, for the next NS simulation domain ($\overline{\Omega}_B \cup \overline{\Omega}_C \cup \overline{\Omega}_D$).
6. Conduct flow simulation in the NS domain ($\overline{\Omega}_B \cup \overline{\Omega}_C \cup \overline{\Omega}_D$), using the HYB3D code, to obtain a converged steady-state solution.
7. Update solution of the whole computational domain.
8. Repeat from Steps 2 to 7 until the maximum number of coupling iterations is exceeded or the preset convergence criterion is reached.

Some specific details in the above procedures are described as follows. In *Procedure 1*, we need to have the most updated solution in the whole domain for determining overlapping regions and interface boundaries between the NS and DSMC solvers. Such solution of the whole domain comes from the “one-shot” HYB3D simulation. Extension of the overlapping regions in *Procedure 2* from Boundary-I towards Boundary-III can slightly increase the computational time in DSMC simulation; however, it may reduce the overall number of coupling iterations required to reach the converged solution according to our numerical experience. Up to four layers of cells in domain $\overline{\Omega}_B$ and two layers of cells in domain $\overline{\Omega}_C$ in the overlapping regions are adopted for quasi-2-D wedge case in the current implementation. The effect of varying the size of overlapping region is reported in Section 3. In *Procedure 4*, the Dirichlet boundary conditions on Boundary-III for the PDSC code are treated according to the Maxwell–Boltzmann velocity distribution assuming that local flow is very close to thermal equilibrium. In *Procedure 7*, the solution of the whole domain is updated as a combination of previous HYB3D and PDSC calculations, with Boundary-II acting as the interface for the solution. In addition, the use of the unstructured mesh is highly justified since the locations of the Boundary-I and -III may not be smooth and have irregular shapes. This often occurs in multi-dimensional flows.

2.2.4. Practical implementation

Numerical simulations with the coupled DSMC–NS code are conducted on a memory-distributed PC cluster system (64 Nodes, dual processors, 2GB RAM per node, Gbit switching hub) running under a Linux operating system. 32 processors are used throughout this study, unless otherwise specified. The PDSC and HYB3D codes are coupled through a simple shell script (Algorithm 3). Thus, the coupled DSMC–NS code is expected to be highly portable among parallel machines with distributed memory. Most importantly, our experience shows that the I/O time related to the switching of solver and read/write files is negligible comparing to the simulation time used by each solver.

3. Results and discussion

3.1. Verification of the coupled DSMC–NS method

3.1.1. Flow and simulation conditions

A supersonic flow past a 2-D wedge of 25° half-angle with a length of 60.69 mm, the same as that in Wang et al. [7], is chosen as the first step to verify the present coupled DSMC–NS method. An equivalent quasi-2-D DSMC simulation is performed with the PDSC code by imposing the Neumann boundary conditions in the spanwise direction (z -coordinate), which is normal to the 2-D wedge. Tests show that 3–4 cells in the z -direction are generally enough to mimic the 2-D flow. The numerical results of the 2-D DSMC simulation is taken as the benchmark values for the verification of the proposed DSMC–NS method. Free-stream conditions for this test case are listed in Table 1. Note the wedge surface has a wall temperature (T_w) of 293.3 K. The Knudsen number based on the length of the wedge and the free-stream conditions is 0.0017.

Table 1
Free-stream conditions in supersonic flow over quasi-2-D 25° wedge

Gas	ρ_∞	U_∞	T_∞	M_∞
N ₂	6.545E – 4 kg/m ³	1111 m/s	185.6 K	4

In the pure DSMC simulation and the DSMC part of the coupled method, variable hard sphere (VHS) [3] model is used to simulate molecular collisions. Constant rotational collision number of 5 is used in the Larsen–Borgnakke model [22] for simulating energy exchange between translational and rotational degrees of freedom. In the NS simulation (pure CFD or part of the coupled method), a CFL number of 100 and a threshold

Table 2
Four simulation sets with various parameters in supersonic flow over quasi-2-D 25° wedge

Set no.	1	2	3	4
Cell layer no. of $\bar{\Omega}_B$	4	2	4	4
Cell layer no. of $\bar{\Omega}_C$	2	1	2	2
$Kn_{max}^{Thr.}$	0.02	0.02	0.04	0.02
$P_{Tne}^{Thr.}$	0.03	0.03	0.03	0.06
Final DSMC cells	~85,000	~71,000	~64,000	~84,000

Table 3
Total computational time (h) with pure NS solver, pure DSMC and coupled method in supersonic flow over quasi-2-D 25° wedge

	Pure NS	Pure DSMC	Coupled DSMC–NS method ^a		
			One-shot NS	DSMC	NS
Total time	3	16	3	12	9

^a 10 Coupling iterations are used in the coupled method for 2-D 25° wedge flow.

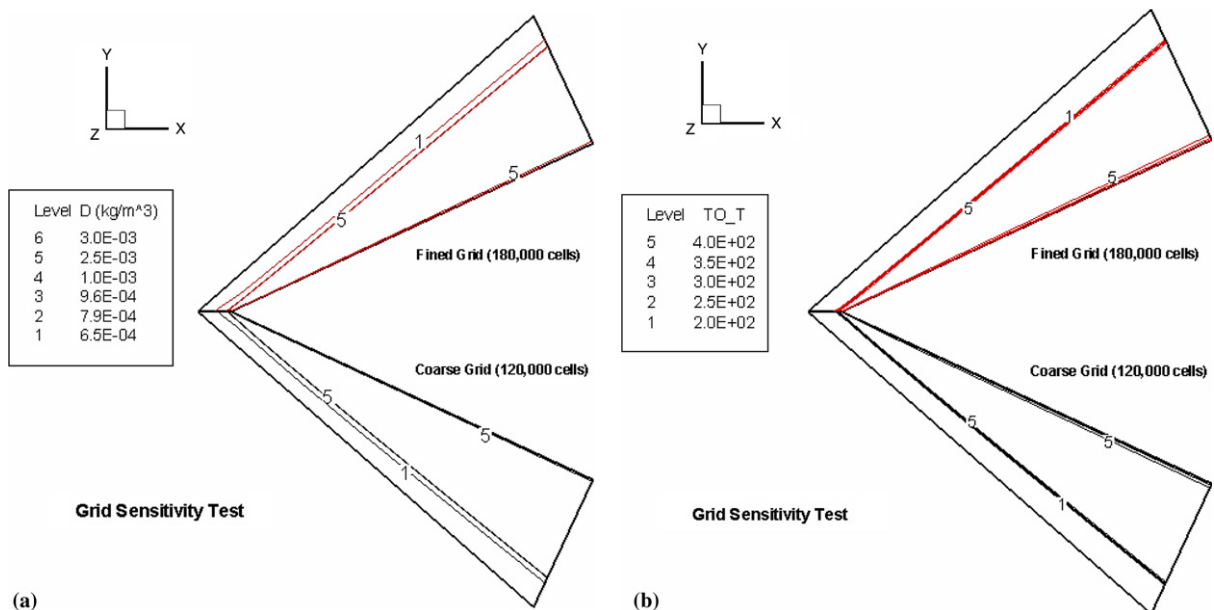


Fig. 3. Grid sensitivity test of HYB3D on quasi-2-D 25° wedge flow: (a) density; (b) total temperature.

parameter of 0.5 in the limiter function proposed by Venkatakrishnan [20] are used throughout this study, unless otherwise specified. The same mesh (180,000 hexahedrons) is used for the three numerical approaches (pure DSMC, pure CFD, and the coupled methods) in the current study. Pure DSMC simulation using the PDSC code is taken as the benchmark result for comparison hereafter in the current test case, since it intrinsically solves the Boltzmann equation that governs the gas flows in all regimes. There are four sets of simulation conditions tested in the current study, which are shown in Table 2. Among those, *Set 1* is taken as the baseline case for future discussions, unless otherwise specified. Also, the parametric details about the different numerical approaches that are used in the current study are presented below.

3.1.1.1. *Pure DSMC simulation and DSMC simulation in the coupled method.* Note that the number appearing in parenthesis in the following description represents the value corresponding to the PDSC simulation in the coupled method. Approximately 3.1 million (0.7 million) particles are used for the pure DSMC simulation.

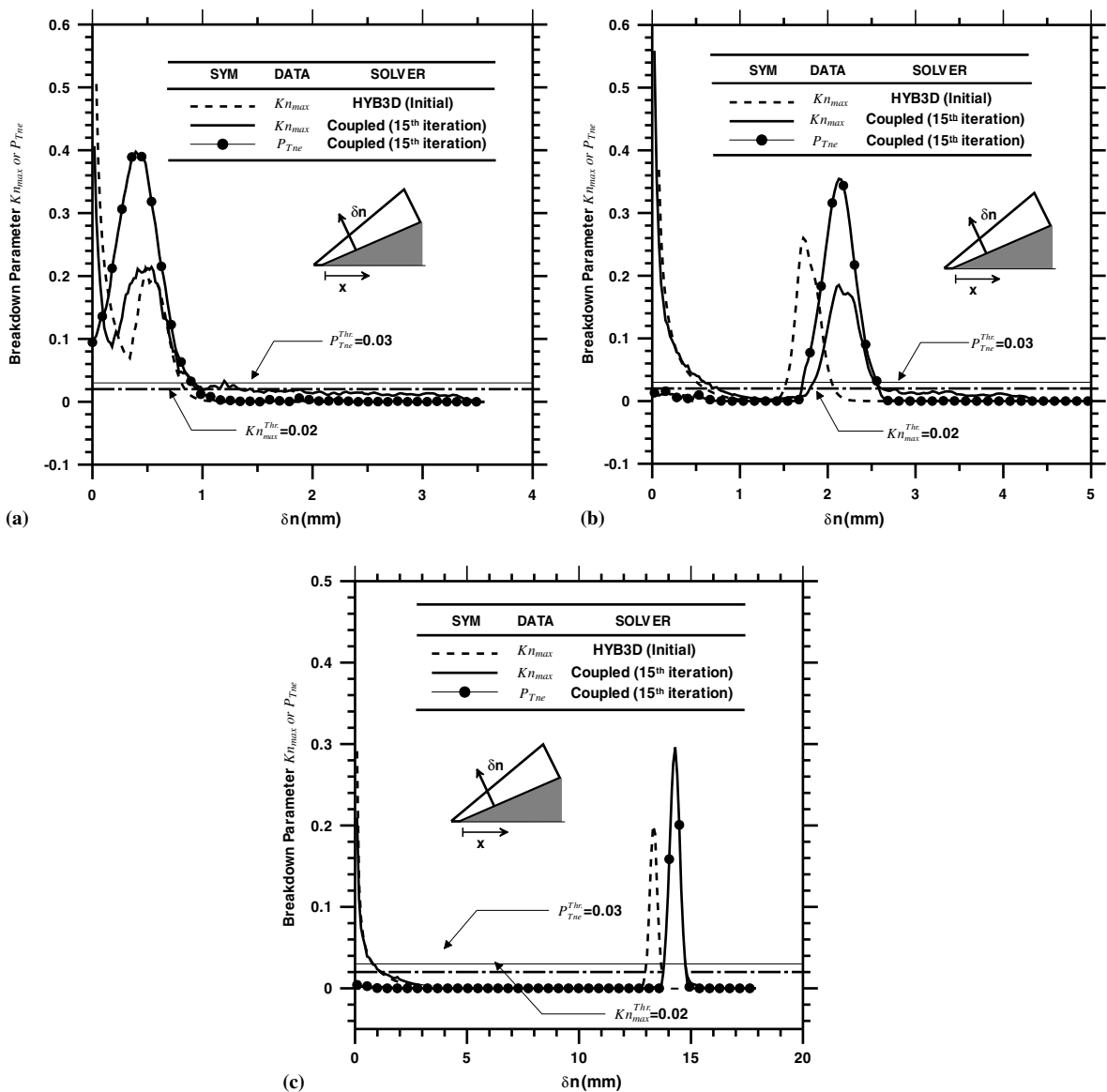


Fig. 4. Breakdown parameters along the line normal to the wedge at: (a) $x = 0.5$ mm; (b) $x = 5$ mm; (c) $x = 50$ mm.

The number of computational cells that are used for PDSC in the coupled method is in the range of 64,000–85,000 (Table 2), which is about 1/3–1/2 of the total number of cells of 180,000 for the pure DSMC method. A number of sampling time steps for the pure DSMC simulation of 35,000 (10,000), and a corresponding number of transient time steps of 30,000 (15,000) are employed to make sure the transient period does not affect the sampling result. The total number of sampling time steps for pure DSMC simulation is much larger than that of DSMC simulation in the coupled method at each iteration step to ensure low statistical uncertainties in the pure DSMC simulation. The reference (or smallest) time step of $8.71E - 9$ seconds is used for both DSMC simulations with the variable time-step approach. The number of particles per cell in the DSMC simulation is generally kept greater than 10 throughout the DSMC simulation domain. Resulting total computational time for the pure DSMC method and DSMC simulation in the coupled method is approximately 16 h and 12 h (for 10 coupled iterations), respectively. Related timing data are also shown in Table 3 for reference.

3.1.1.2. *Pure NS simulation and NS simulation in the coupled method.* In both NS simulations, an implicit scheme with a local time stepping and a CFL number of 100 is used for the time iterations. Iteration numbers of 7000 and 2000 are used for pure NS simulation and NS simulation in the coupled method, respectively. In addition, grid convergence of the NS code is demonstrated in Fig. 3, where the simulated data using fewer cells

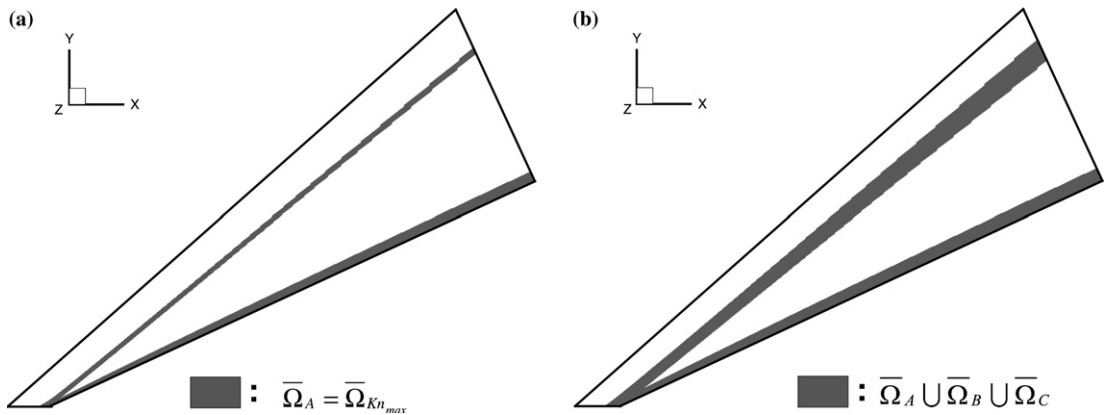


Fig. 5. Initial domain distribution in quasi-2-D 25° wedge flow: (a) continuum breakdown domain; (b) DSMC domain including the overlapping regions.

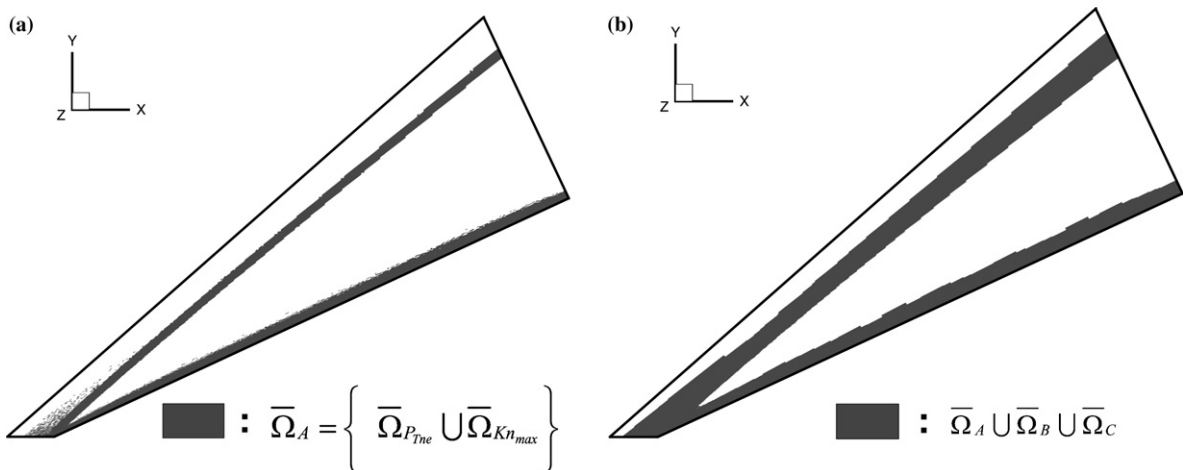


Fig. 6. Domain distribution at 15th coupling iteration in quasi-2-D 25° wedge flow: (a) breakdown domain; (b) DSMC domain including the overlapping regions.

(120,000 cells) are essentially the same as those by (180,000 cells) as used in the verification of the coupled method with the quasi-2-D wedge flow. In the current study, 180,000 cells are used throughout the study, unless otherwise specified. The number of computational cells for HYB3D in the coupled method is about 1/2–2/3 of the total number of cells used for pure NS simulation. Total HYB3D computational time is approximately 3 h and 9 h (for 10 coupling iterations), respectively, for the pure NS simulation and the NS simulation in the coupled method. Furthermore, the total computational time in the coupled method is about 24 h (Table 3). For other sets of simulation, the total computational time of the coupled method is within $\pm 20\%$ difference from that of Set 1 simulation.

3.1.2. Distribution of breakdown parameters

The distributions of breakdown parameters of test case Set 1 (initial values of Kn_{\max} , and Kn_{\max} and P_{Tne} at the end of 15th coupled iteration) along the normal direction from the wedge surface at $x = 0.5, 5$ and 50 mm are illustrated in Fig. 4a–c, respectively. As discussed before, only the DSMC method is able to produce P_{Tne} ; hence, there is no corresponding distribution of the thermal non-equilibrium indicator after the initial HYB3D simulation. Two horizontal lines showing the threshold values (0.02 for Kn_{\max} and 0.03 for P_{Tne}) become the borderlines that continuum breaks down or thermal non-equilibrium exists, in which the NS solver cannot be used. General trend of the Kn_{\max} distribution along the normal direction from the wedge surface shows that the value is rather large (up to 0.4 or larger) near the surface ($x = 0.5, 5$ mm) due to large property gradients in the viscous boundary layer, and then decreases to a much smaller value in the region between the boundary layer and the oblique shock, and finally becomes large again across the oblique shock (slightly larger than 0.2 or less). As for the P_{Tne} distribution, high value (up to 0.4) can be found only at the location across the oblique shock at all surface locations. Noticeably, a comparably broader region for P_{Tne} than Kn_{\max} can be found in Fig. 4a–b, which justifies the use of the thermal non-equilibrium indicator, P_{Tne} , in the current study. In addition, the maximum value of Kn_{\max} across the oblique shock decreases slightly with increasing distance from the leading edge. This is understandable since the property gradient near the leading edge is very large. Another important finding is that the initial distribution of Kn_{\max} , computed from the initial HYB3D simulation, differs to a great extent from that after the final (15th) coupling iteration. This shows that previous “one-shot” CFD simulation, which provides the Dirichlet-type boundary conditions for the DSMC simula-

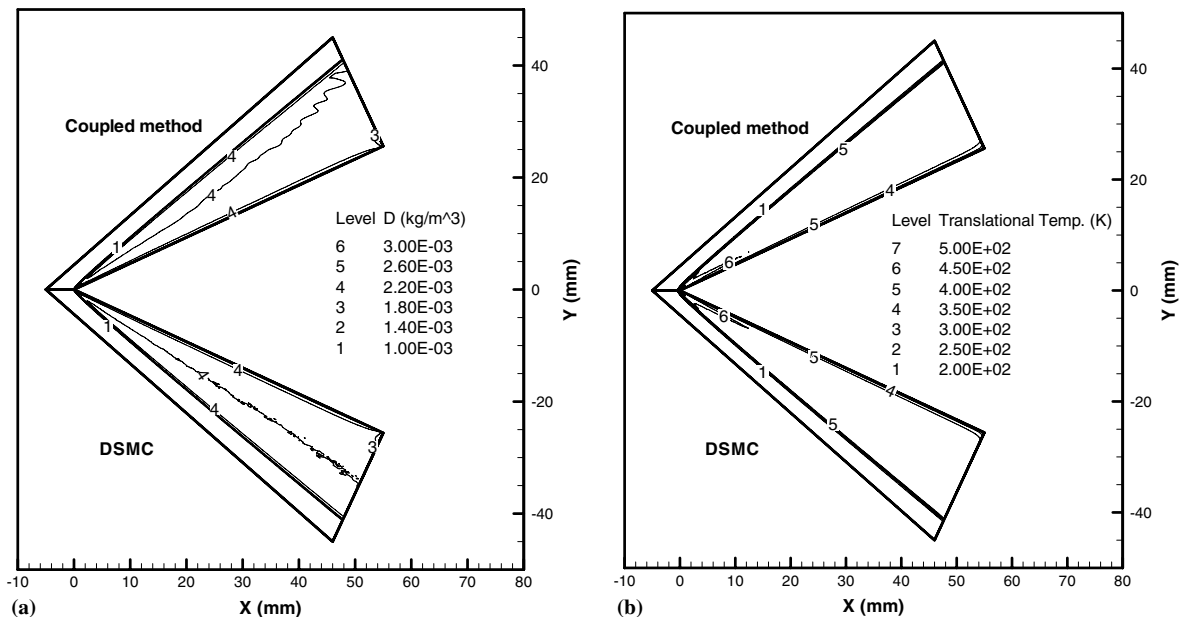


Fig. 7. Properties comparison between the DSMC method and the present coupled DSMC–NS method in quasi-2-D 25° wedge flow: (a) density; (b) translation temperature.

tion, is problematic for an accurate simulation. Also, the maximum values of Kn_{max} , predicted by the latest PDSC simulation, are generally lower than those predicted by the initial HYB3D simulation except the leading edge region. Based on the distribution of breakdown parameters calculated at each iteration step, the threshold value of breakdown parameters and the concept of overlapping regions mentioned earlier, the proposed coupled DSMC–NS method thus properly determine the computational domain for the DSMC and NS solvers, respectively.

3.1.3. Evolution of DSMC and NS domains

Fig. 5a and b, respectively, shows the initial distribution of continuum (NS) breakdown regions ($\bar{\Omega}_A$) and DSMC simulation domains ($\bar{\Omega}_A \cup \bar{\Omega}_B \cup \bar{\Omega}_C$) in the coupled method, while Fig. 6a and b, respectively, shows the corresponding distribution after the 15th coupled iteration. Note that the initial distribution of NS breakdown regions is solely determined by the HYB3D computation for the whole domain, while the later

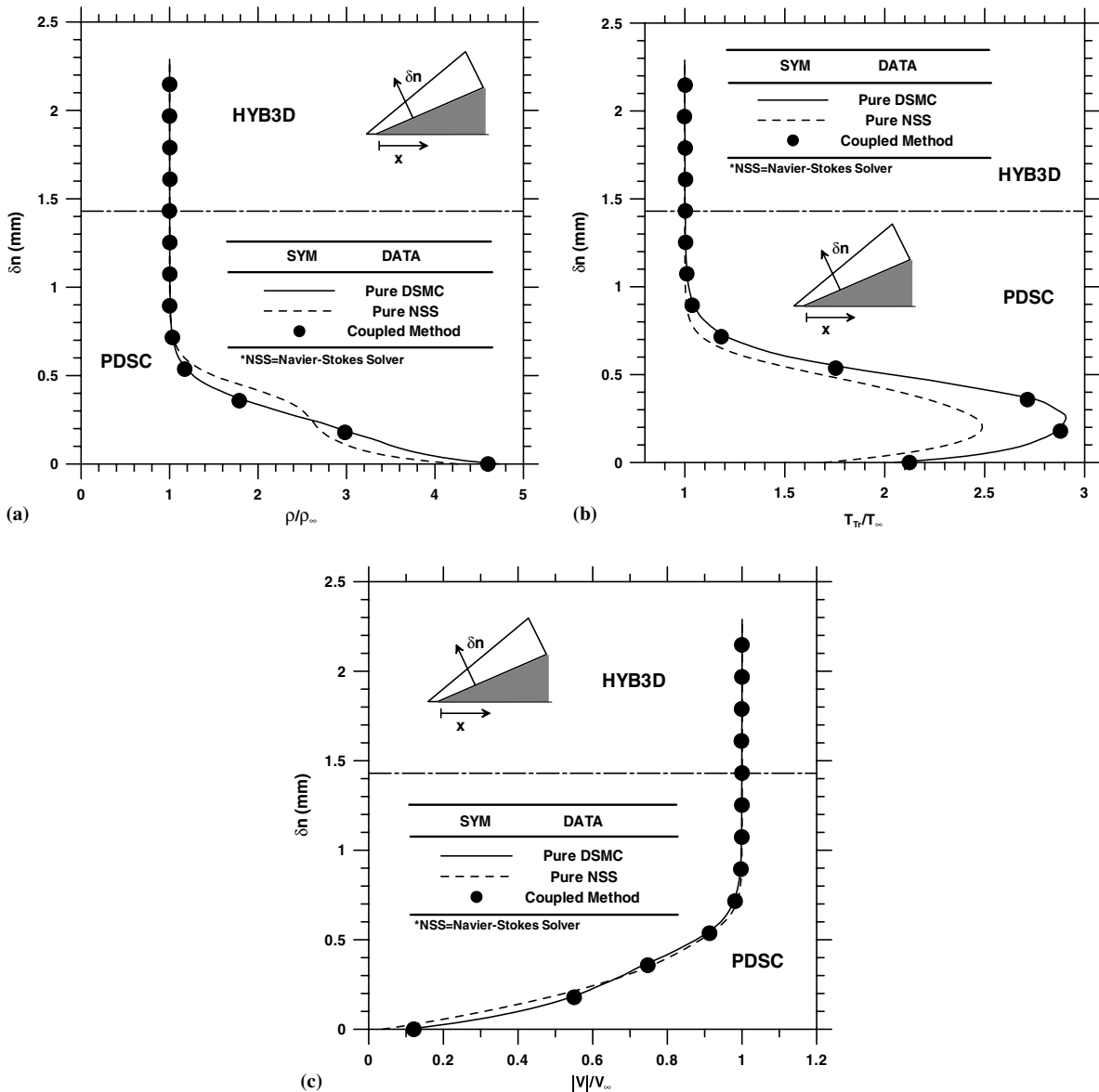


Fig. 8. Properties profile along a line normal to the wedge at $x = 0.5$ mm: (a) density; (b) translational temperature; (c) velocity.

distribution is updated from the solutions of both PDSC and HYB3D simulations. In Fig. 6a, the continuum breakdown regions are rather scattered, especially near the leading-edge region, while in Fig. 6b the DSMC simulation domains that are originally disconnected spatially becomes connected due to the current strategy of overlapping regions. In the current test case, there are two major DSMC simulation domains: one is across the oblique shock and the other is near the boundary layer of the wedge surface. In addition, the region in front of the leading edge is also identified as the DSMC simulation domain due to large gradient of the flow properties. To be numerically accurate, a threshold value of Kn_{\max} in the current study is chosen conservatively as 0.02, which guarantees that even minor deviation from the continuum theory can be captured. Note that Wang et al. [7] used the same value, although Wang and Boyd [21] previously recommended 0.05 as the threshold value instead. Consideration of another breakdown parameter P_{Tne} (0.03 in the current study) further extends the possible DSMC simulation region, especially in the region near the leading edge and across the oblique shock, as can be seen in Fig. 4a–c. Thus, we can expect a larger DSMC domain exists,

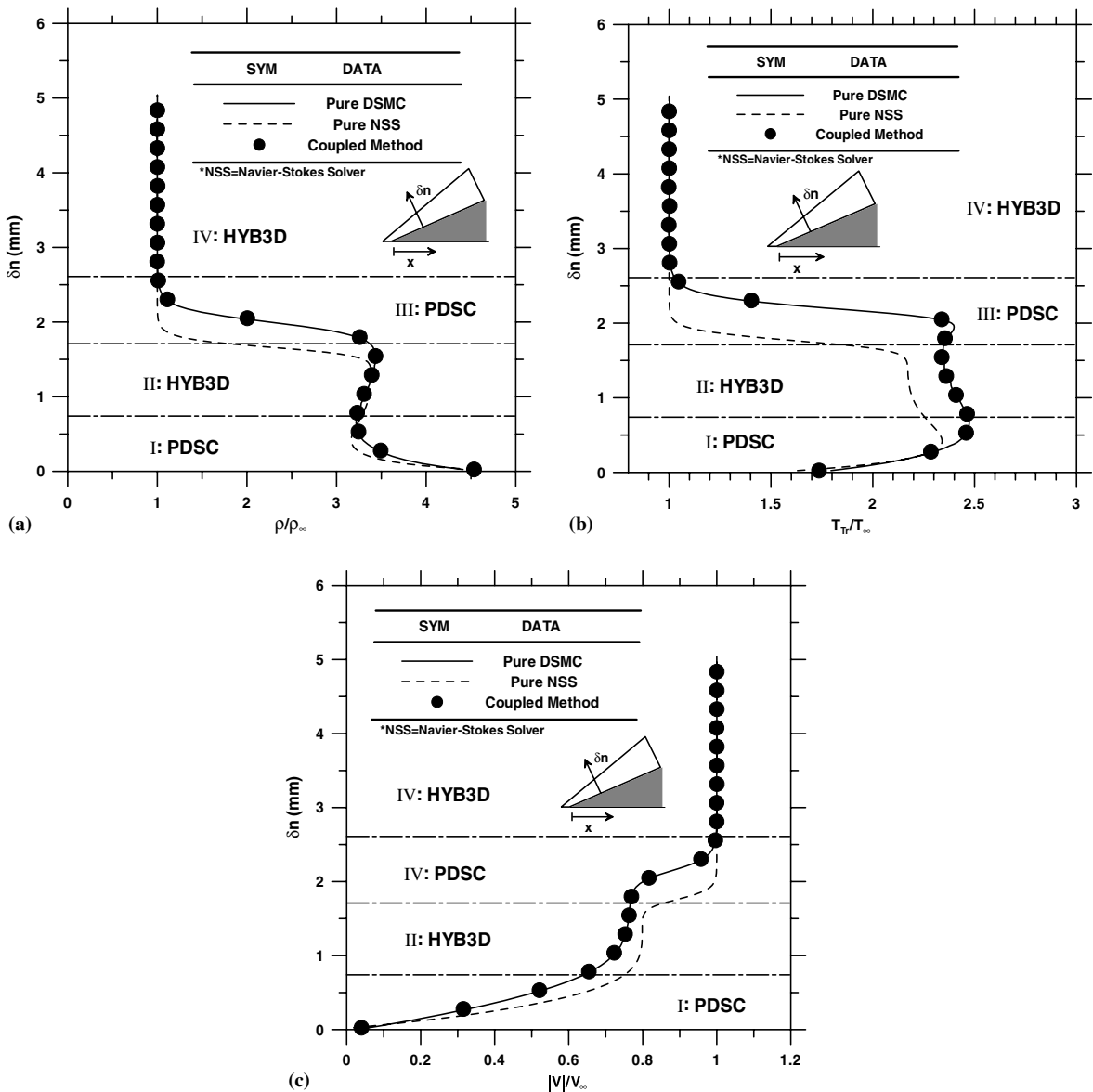


Fig. 9. Properties profile along a line normal to the wedge at $x = 5$ mm: (a) density; (b) translational temperature; (c) velocity.

which increases the computational time accordingly, should this threshold value decrease even more. Of course, both Kn_{max} and P_{Tne} can be adjusted based on numerical experience. Comparing Fig. 5 with Fig. 6, we can find that the DSMC simulation domain expands with increasing number of coupled iteration, which justifies the necessity of repeated coupling between two solvers as proposed in the current study. Nevertheless, the DSMC simulation region ceases to expand as the converged solution is reached.

3.1.4. Comparison of the coupled DSMC–NS method with the pure DSMC method

Figs. 7a and b compare contour distributions of density and translational temperature, respectively, obtained from the pure DSMC simulation and the coupled DSMC–NS method. The results of the present coupled DSMC–NS method are in excellent agreement with those of pure DSMC simulation except the unexpected density profile behind the oblique shock near the downstream end. Note that the wiggle appearing in Fig. 7a (density contour) may be misleading at first glance since the density values in the region between the

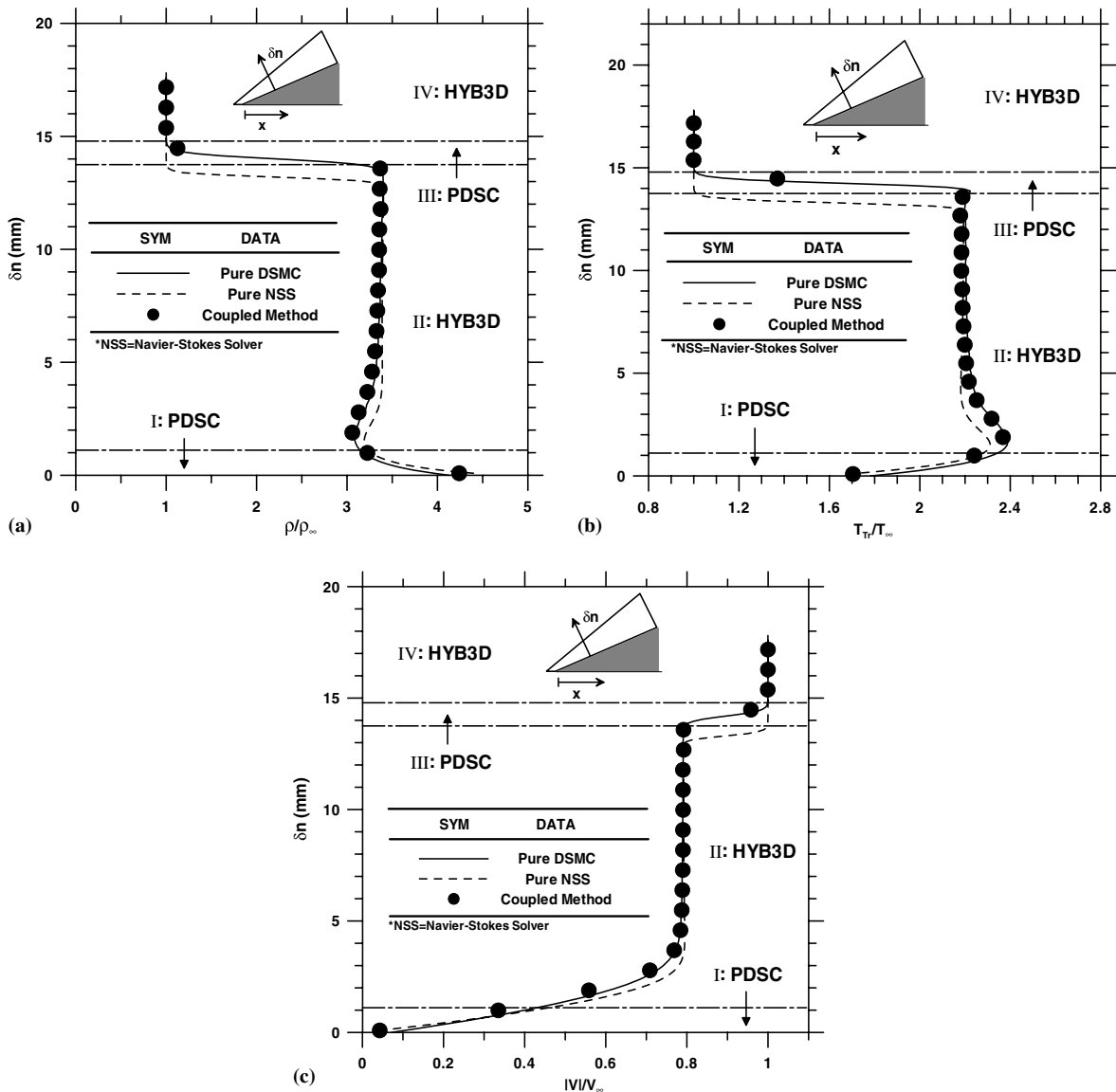


Fig. 10. Properties profile along a line normal to the wedge at $x = 50$ mm: (a) density; (b) translational temperature; (c) velocity.

oblique shock and the wedge surface is actually almost uniform. Obviously, the oblique shock originating from the leading edge is well captured by both pure DSMC simulation and the coupled method. Detailed comparisons of density and temperature profiles obtained from the present coupled DSMC–NS, pure DSMC and pure NS solvers are introduced next to further demonstrate the validity of the current proposed coupled DSMC–NS method.

Fig. 8a–c shows the comparison of density, temperature and velocity contour, respectively, obtained from these three numerical methods, along a line normal to the wedge surface (δn direction) at $x = 0.5$ mm. Horizontal dash-dot line represents the boundary between the NS solution domain (above) and the DSMC solution domain (below). In addition, the data of the coupled method represent the results after the 15th coupled iteration. Due to rarefaction of the free stream and the shock forming near the leading edge region, as shown in those figures, the majority portion normal to the wedge surface at this location belongs to the DSMC sim-

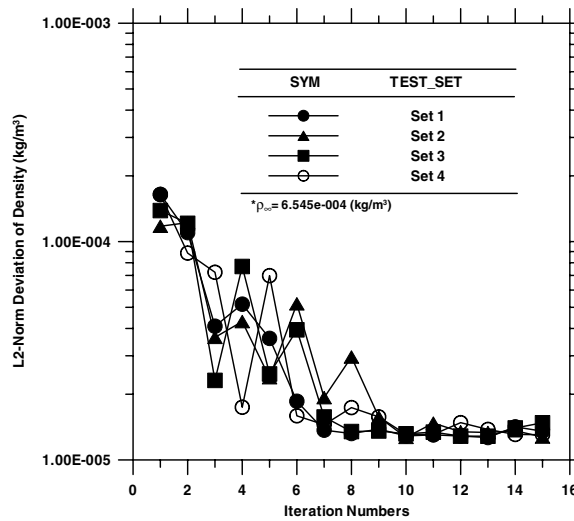


Fig. 11. Convergence history of L2-norm deviation of density among the four simulation sets in quasi-2-D 25° wedge flow.

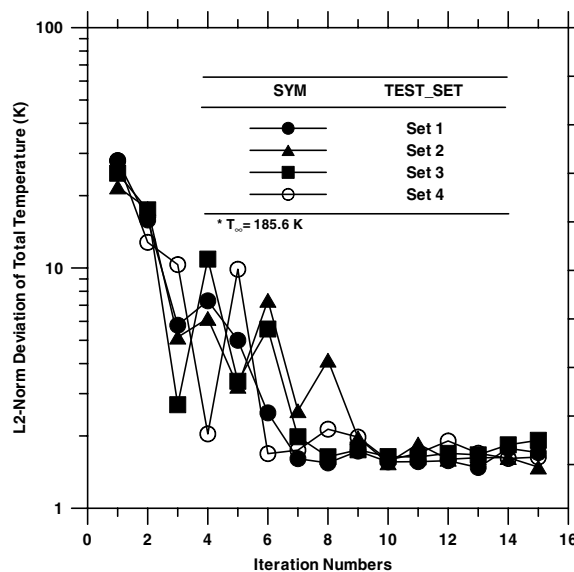


Fig. 12. Convergence history of L2-norm deviation of total temperature among the four simulation sets in quasi-2-D 25° wedge flow.

ulation domain except for the region far away from the wedge surface (large δn). Results of the coupled method are in excellent agreement with those of pure DSMC simulation at all δn of $x = 0.5$ mm. Because the HYB3D code only solves the thermal-equilibrium and continuum-based governing equations, the results of HYB3D are different to a large extent from other two methods due to the combined effect of large Kn_{max} (low density and large gradient of properties) and large P_{Tne} (highly thermal non-equilibrium) near the leading edge. Observation from Fig. 8a–c shows that overlapping regions may be shrunk to further reduce the computational time. Effects of reducing the overlapping regions are discussed later.

Fig. 9a–c shows the similar comparison among the three numerical approaches at $x = 5$ mm. Based on the calculated breakdown parameters (Kn_{max} and P_{Tne}) and the selected threshold values, the flow region is divided into four sub-domains along the δn direction, as shown in Fig. 9: Zone I ($\delta n < 0.74$ mm) and Zone III (1.71 mm $< \delta n < 2.61$ mm) are the DSMC solution domains, while the other two regions, Zone II (0.74 mm $< \delta n < 1.71$ mm) and Zone IV ($\delta n > 2.61$ mm), are the NS solution domains. At this location, the results of the NS solver deviate appreciably from those of both pure DSMC simulation and the coupled method. This deviation occurs even in the region between the shock and the boundary layer, where it is identified as the NS solution domain. This large deviation is reasonable since the boundary conditions for the NS solution domain (Zone II) can only be accurately obtained from DSMC simulation domains (Zones I and III). Results of the present coupled method are still in excellent agreement with those of pure DSMC simulation for the entire domain.

Fig. 10a–c also shows the similar comparison among the three numerical methods at $x = 50$ mm, which is very close to the outflow boundary in the current test case. The flow region is again divided into four sub-domains along the δn direction. Two zones (I and III) are the DSMC simulation domains, while the other two zones (II and IV) are the NS simulation domains. In general, similar trends to Fig. 9 can still be found in Fig. 10 except that there is a slight discrepancy between the coupled method and pure DSMC simulation. This could be possibly due to the problematic treatment of outflow boundary conditions in the DSMC simulation. In the NS simulation, supersonic outflow boundary conditions assuming no information is passed back to the computational domain from the outside, while in DSMC simulation, fixed outflow boundary conditions based on free-stream supersonic flow conditions are used, which are obviously incorrect. Indeed, further detailed study regarding this matter is required to resolve the discrepancy.

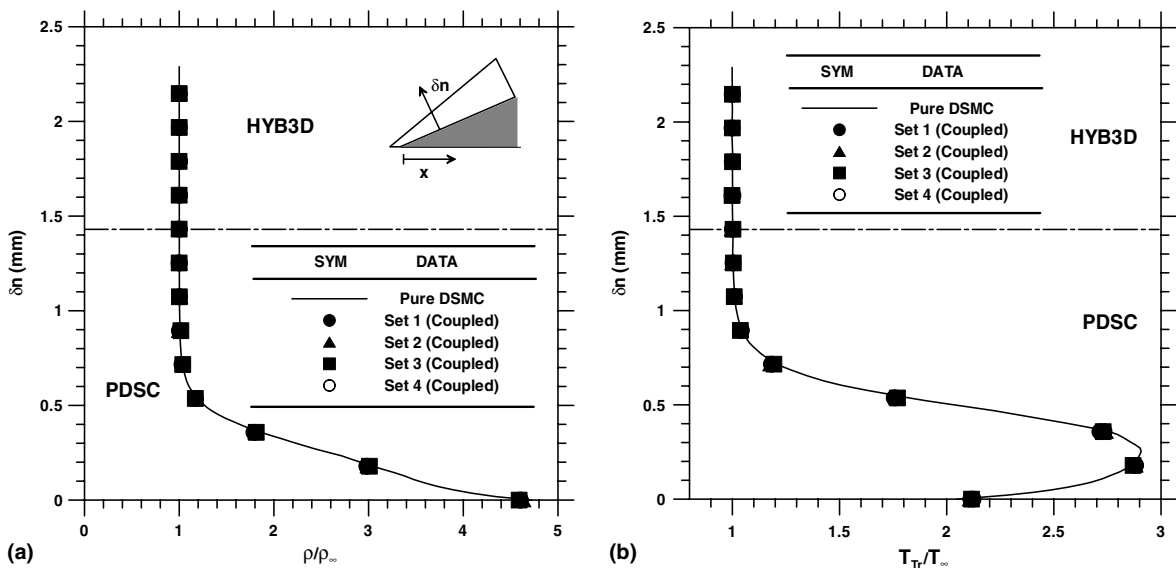


Fig. 13. Comparison of properties along a line normal to the wedge at $x = 0.5$ mm among the four simulation sets: (a) density; (b) translational temperature.

3.1.5. Effect of varying simulation parameters on convergence

As mentioned earlier, varying the size of the overlapping regions and the criteria of breakdown parameters may have an impact on the convergence rate, computational cost and accuracy of solutions. Figs. 11 and 12 illustrate the convergence history of L2-norm deviation of density and total temperature, respectively, with different simulation parameters. This L2-norm deviation for i th iteration is defined as the root mean square of flow properties between the $(i - 1)$ th and the i th iteration in the whole simulation domain. There are 4 test sets of simulation conditions listed in Table 2. Note that the L2-norm deviations level off within less than 10 coupled iterations for all the test sets. Indeed, the converged deviation of flow properties depends upon the statistical uncertainties of the DSMC solver [4]. However, the effect of the number of sampling used in the PDSC code is not pursued in the current study. As compared with the baseline case (Set 1), decreasing the size of overlapping regions (Set 2) or increasing the threshold values of $Kn_{max}^{Thr.}$ (Set 3) and $P_{Tne}^{Thr.}$ (Set 4) does not clearly change the convergence behavior of the coupled method as shown in Figs. 11 and 12. In addition, varying the simulation parameters (Set 1–Set 4 in Table 2) does not alter the accuracy of the solution. Typical examples are shown in Fig. 13a and b ($x = 0.5$ mm), whereas the profiles of flow properties at other positions show a similar trend. However, the choice of simulation parameters slightly changes the resulting number of cells for DSMC simulation (Table 2), which in turn may change the total computational time slightly. In addi-

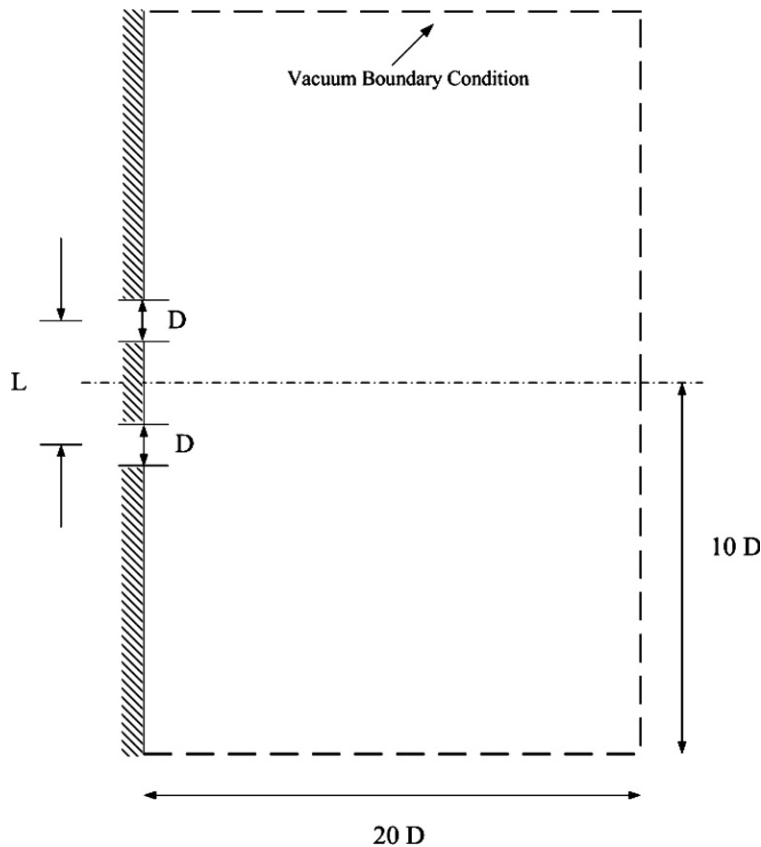


Fig. 14. Sketch of two parallel near-continuum orifice free jets flow.

Table 4
Sonic conditions at the orifice exiting plane in two parallel near-continuum orifice free jets flow

Gas	ρ_{throat}	U_{throat}	T_{throat}	Re_{throat}
N ₂	6.52E - 3 kg/m ³	314 m/s	237.5 K	401

tion, this slightly large number of coupled iterations required for convergence will be discussed in detail next along with the results by applying the coupled method in computing a 3-D realistic flow.

3.2. 3-D application of the coupled DSMC–NS method

To demonstrate the present coupled DSMC–NS method in dealing with realistic 3-D flows, a nitrogen flow with two parallel near-continuum orifice jets issuing into a near-vacuum environment is simulated. This flow is in generally very difficult to simulate alone using either the DSMC or NS solver.

Fig. 14 schematically shows two parallel near-continuum thin orifice free jets (nitrogen gas, orifice diameter = 3 mm, distance of two orifice centers = 9 mm) issuing into a near-vacuum environment. This flow has been experimentally measured by Soga [28] with background pressure ~3.7 Pa. Since only limited computational domain is utilized, vacuum boundary conditions are employed at all outer boundaries for simplicity. In addition, only 1/4 of the whole physical domain is simulated due to the geometrical symmetry. Inflow conditions at the thin orifices, as summarized in Table 4, are assumed to be sonic with flow data obtained from 1-D inviscid flow analysis. Indeed, this restriction can be relieved if a pressure-based NS solver, unlike the current

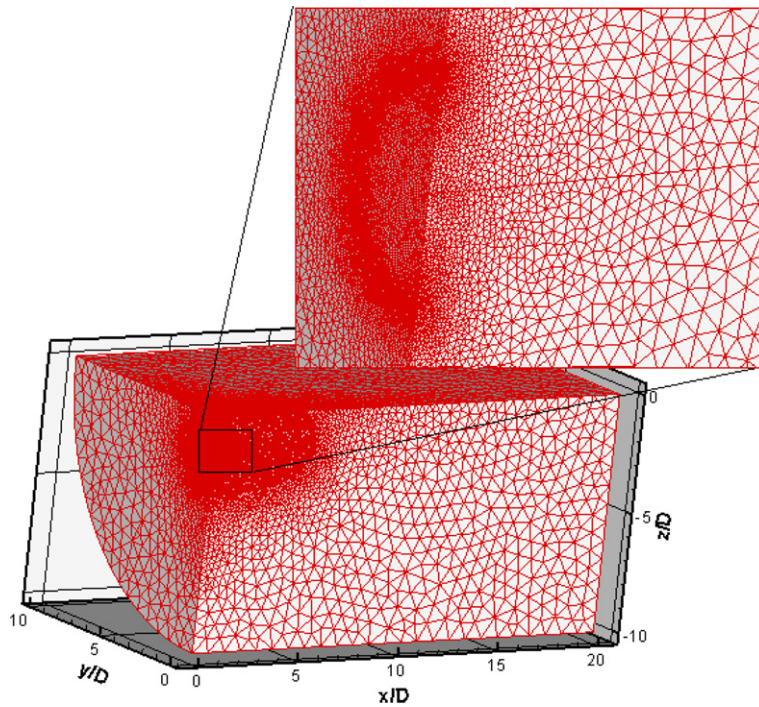


Fig. 15. Mesh distribution of two parallel near-continuum orifice free jets flow simulation.

Table 5
 Simulational conditions of two parallel near-continuum orifice free jets flow

Method	DSMC for coupled method ^a
Cell no.	~470,000
Simulated particle no.	~6,200,000
Reference Δt (s)	3.01E – 09
Sampling time steps	13,500
Cell layer no. of $\bar{\Omega}_B$	1
Cell layer no. of $\bar{\Omega}_C$	0
$Kn_{\max}^{\text{Thr.}}$	0.05
$p_{\text{Tne}}^{\text{Thr.}}$	0.1

^a Total cell no. of computational domain for coupled DSMC–NS method is 520,830.

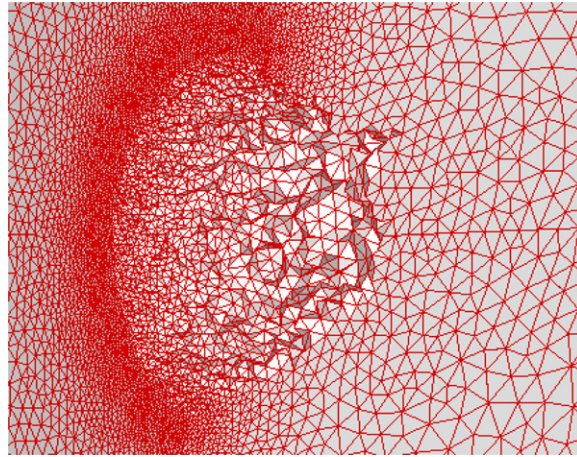


Fig. 16. Surface mesh distribution of breakdown domain (DSMC domain) of two parallel near-continuum orifice free jets flow simulation with an exploded view.

Table 6

Total computational time (h) with pure NS solver and coupled method in two parallel near-continuum orifice free jets flow

	Pure NS	Coupled DSMC–NS method ^a		
		One-shot NS	DSMC	NS
Total time	2.5	2.5	22.5 31	4

^a 3 Coupling iterations are used for a converged solution in the coupled method.

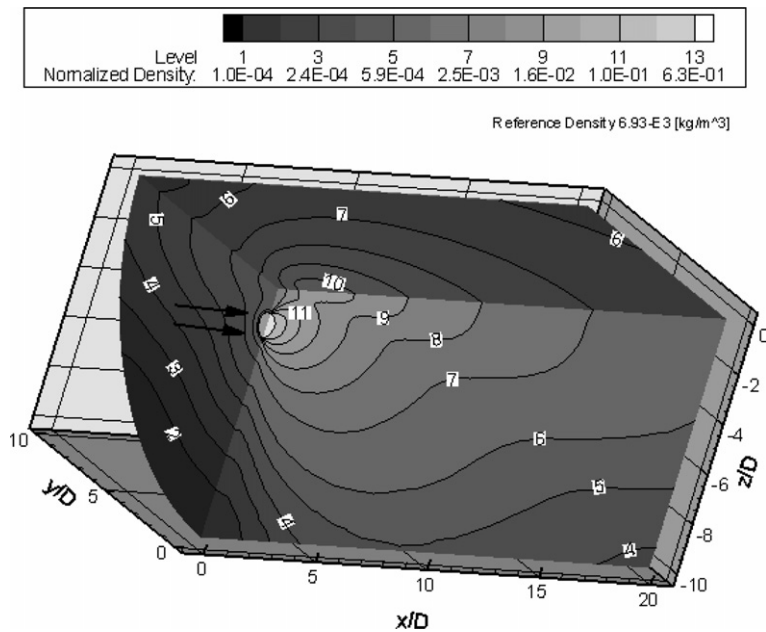


Fig. 17. Density contour of two parallel near-continuum orifice free jets flow.

HYB3D code, is selected that can be used to simulate starting from the stagnation reservoir. Clearly, this flow is too dense for a meaningful DSMC simulation based on the flow conditions at the orifices ($Kn_{throat} = 0.00385$), while it is too rarefied for a correct NS simulation due to the near-vacuum ambient environment.

Fig. 15 shows the global surface mesh distribution, which is used for the coupled method, along with an exploded view of the surface mesh distribution near the orifice. Note only tetrahedral mesh is used in this simulation. Computational domain extends up to 20D, 10D and 10D, respectively, in the direction of x - (streamwise), y - (crosstreamwise) and z -coordinate (crosstreamwise). Mesh near the orifice lip is intentionally refined considering the large gradient of flow properties in this region. Resulting number of cells is approximately 0.52 million, while other simulation conditions are summarized in Table 5. Among these, Kn_{max}^{Thr} and P_{Tne}^{Thr} are chosen as 0.05 and 0.1, respectively. One cell layer is used for $\bar{\Omega}_B$, and none for $\bar{\Omega}_C$. In addition, at all outer boundaries supersonic flow boundary conditions and vacuum boundary conditions are assumed, respectively, in the NS and DSMC solver. Fig. 16 illustrates the exploded view of the surface mesh distribution of DSMC domain

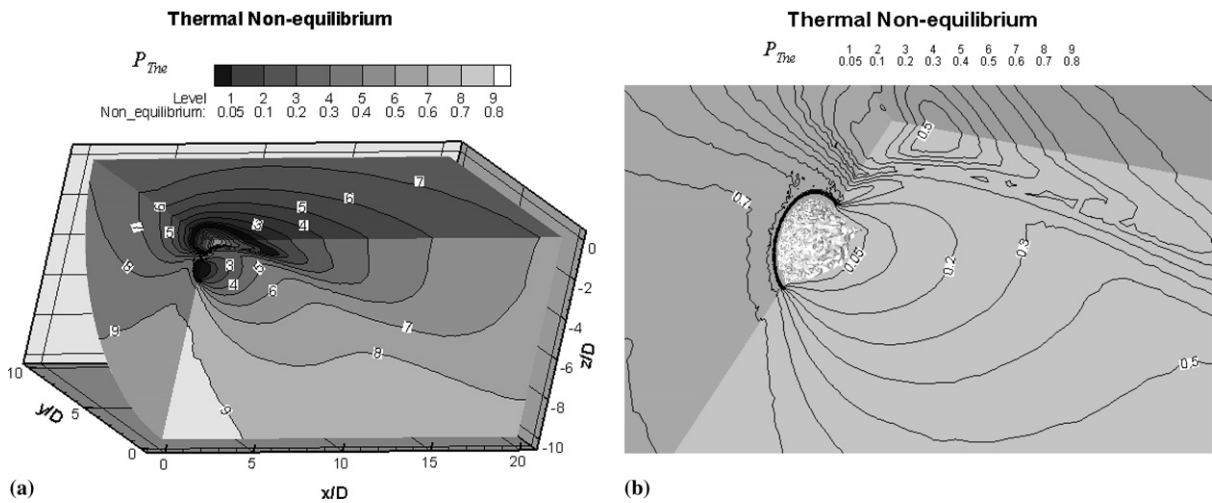


Fig. 18. Thermal non-equilibrium contour of two parallel near-continuum orifice free jets flow: (a) on the global surface; (b) near the orifice.

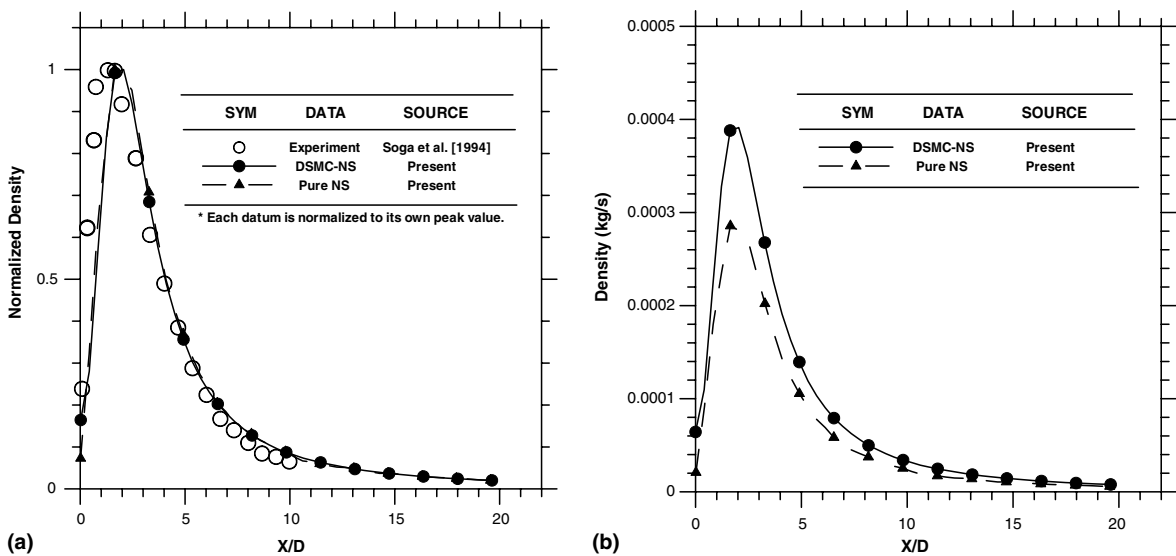


Fig. 19. Normalized density distribution along the symmetric line of two parallel near-continuum orifice free jets flow.

(breakdown region) in the coupled method after 2nd iteration. Related timing data are also shown in Table 6 for reference.

Fig. 17 illustrates the density contour distribution at the symmetric and orifice planes. In each orifice jet, the flow expands very quickly into the near-vacuum environment, while at the symmetric line between two orifice jets a secondary jet is clearly formed due to the expanding molecules from both jets. Fig. 18a illustrates the contour distribution of thermal non-equilibrium (P_{Tne}) at the symmetric and orifice planes, while Fig. 18b shows the contour distribution of thermal non-equilibrium near the orifice with the surface of the breakdown domain in the enlarged view. It clearly shows that except near the entrance of the orifice jet most regions are highly non-equilibrium, which necessitates the use of DSMC solver. The region simulated by the NS solver is considerably small; however, it becomes a formidable task using the DSMC solver alone at this low Knudsen number (0.00385).

Figs. 19 and 20, respectively, illustrate the simulated profile of density and rotational temperature along the symmetric line between the two jets, along with pure NS data and experimental data [28]. It should be noted

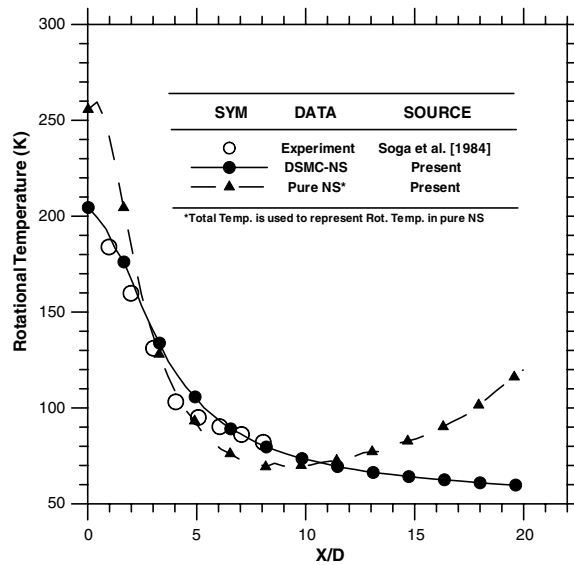


Fig. 20. Rotational temperature distribution along the symmetric line of two parallel near-continuum orifice free jets flow.

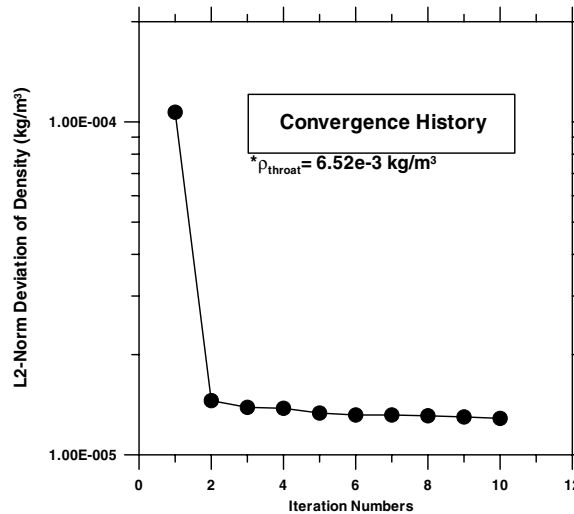


Fig. 21. Convergence history of density for two parallel near-continuum orifice free jets flow.

that since only normalized density data were provided in Ref. [28], comparisons of normalized densities (with respect to their corresponding peak values) between hybrid, pure NS, and test data are made in Fig. 19a. Thus, Fig. 19a serves to demonstrate the general trend of both predictions (hybrid and pure NS) coincide with the measured data, except in the near-wall region. However, the absolute densities predicted by both methods differ substantially because the values of continuum breakdown parameters are large (>0.05) along this symmetric line, where there is a large gradient of flow properties in the near field and strong rarefaction in the far field. This phenomenon can be clearly seen in Fig. 19b. Results show that density first increases very rapidly with increasing x/D , then reaches a maximal value near $x/D = 2$ due to the collisions of gas molecules from both jets and finally decreases rapidly towards ambient value. In contrast, temperature decreases continuously from ~ 200 K at $x/D = 0$ with increasing x/D . Note only the total temperature obtained in the pure NS method is presented due to the assumption of thermal-equilibrium in the NS solver (HYB-3D). In this highly rarefied region, the simulated temperature data using coupled method agree reasonably well with experimental data within experimental uncertainties, while the temperature data by NS solver deviate greatly from experimental data as expected. In addition, the simulation data of the coupled method deviate relatively large from the

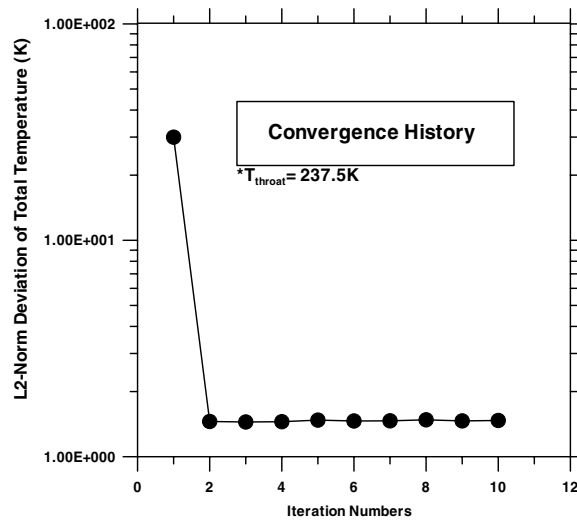
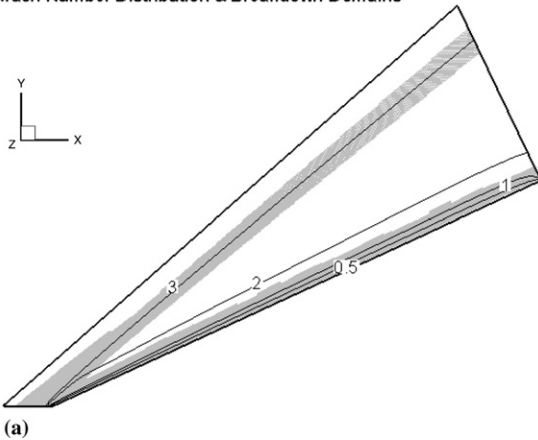


Fig. 22. Convergence history of total temperature for two parallel near-continuum orifice free jets flow.

Mach Number Distribution & Breakdown Domains



Mach Number Distribution near the Orifice

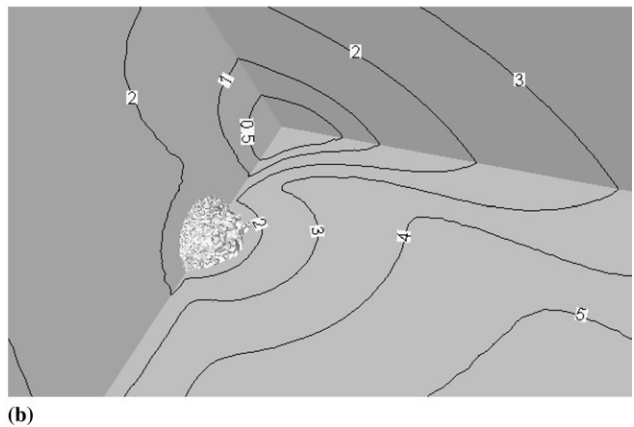


Fig. 23. Mach number distribution near the breakdown interfaces: (a) quasi-2-D supersonic wedge flow; (b) two parallel near-continuum free jets.

experimental data near the wall region ($x/D \leq 1$), which requires further investigation. There are two possible reasons of this large deviation. One is that it might originate from the errors introduced by reflection of light from the wall in Soga's study using fluorescence technique [28]. Another possible reason is the inlet flow data assuming 1-D inviscid flow conditions.

Figs. 21 and 22 show the convergence history of the L2-norm deviation of density and temperature, respectively. The density deviation decreases from $1.1E - 4 \text{ kg/m}^3$ down to $1.3E - 5 \text{ kg/m}^3$ and levels off quickly after two coupling iterations, while the temperature deviation shows similar trend decreasing from 30 K down to ~ 1.5 K. This fast convergence of the deviation as compared to the case of quasi-2-D wedge flow can be clearly explained by Fig. 23, which shows the Mach number contour distribution near the breakdown interface for both cases of quasi-2-D wedge flow and of two parallel jets. In Fig. 23a subsonic flow dominates in the regions near the breakdown interface above the boundary layer along the wedge wall that necessitates more number of couplings to exchange the information between two solvers, although supersonic flow dominates in the regions near the breakdown interface around the oblique shock. However, in Fig. 23b, supersonic flow dominates near the breakdown interface around entrance regime of orifice jets, which greatly reduces the number of couplings required for convergence as seen from the simulation. The above observation is very important from the viewpoints of practical implementation. For example, in the early stage of simulation we can determine the number of couplings required for convergence by simply monitoring to which the flow regime (supersonic or subsonic) near the breakdown interface belongs. If most flows near the breakdown interface are supersonic, then two coupling iterations should be enough for convergence. If not, more coupling iterations (e.g. less than ten) are required to have a converged solution. Further investigation in determining the optimum number of coupling iterations is required in practical applications of the current coupled method.

4. Conclusions

A coupled DSMC–NS approach using 3-D unstructured mesh is presented to combine the high computational efficiency of the NS solver in continuum and thermal-equilibrium regions with high fidelity of the DSMC method in “breakdown” regions. Flexible overlapping regions between DSMC and NS simulation domains are designed by taking advantage of the unstructured grid topology in both solvers. Two breakdown parameters, including a continuum breakdown parameter proposed by Wang and Boyd [21] and a thermal non-equilibrium indicator, are employed to determine the DSMC simulation and NS simulation domains, in addition to the concept of overlapping regions. The results from a pure DSMC simulation of a supersonic flow past a quasi-2-D wedge case is chosen as the benchmark data for evaluating and verifying the present coupled method. In addition, a realistic 3-D nitrogen flow, which two parallel near-continuum orifice jets expands into a near-vacuum environment, is simulated to demonstrate the capability of the current coupled method in dealing with practical problems. The present coupled DSMC–NS method is shown to be capable of accurately simulating the characteristics of the continuum and thermal-equilibrium breakdown in the test cases. It is argued that the present coupled approach using flexible overlapping regions can be easily applied to any DSMC and NS solvers using the unstructured grid topology in general. Nevertheless, the advantage of applying this coupled method to simulate flow, which is predominantly continuum, can be highly expected since the computation with the pure DSMC method is practically impossible and the pure NS solver is incorrect in rarefied regions.

Though successful results for the test cases were obtained from the present coupled approach, extensive studies with other more challenging 3-D test cases in the future are needed to further verify the present approach. Some comments about extending the current coupling method are made as follows. First, a thermal-equilibrium NS solver, HYB3D, is chosen in the current study and cannot correctly model the region involved with thermal non-equilibrium phenomena. The DSMC domain needs to cover not only continuum breakdown but also thermal non-equilibrium regions, in which the use of a multiple-temperature NS solver is more appropriate. Hence, it may be justified to either use a multiple-temperature NS code, or implement the multiple-temperature capability into HYB3D to promote the computational efficiency by simulating thermal non-equilibrium region without using DSMC. Second, an implicit scheme with a CFL number of 100 is used in the current NS solver while the time step of DSMC is constrained by the limit of a unity CFL number time step. Thus, it is highly possible that the coupling between DSMC and NS solvers can be made at each NS time

step, over which DSMC data are accumulated for 100–1000 DSMC time steps. If a sufficiently large number of simulation particles in DSMC can be used along with possible “multi-level” cloning technique [8], then a fairly low-noise coupling between DSMC and NS solver for unsteady flows may be performed, although its cost is expected to be high as compared to steady-flow simulation.

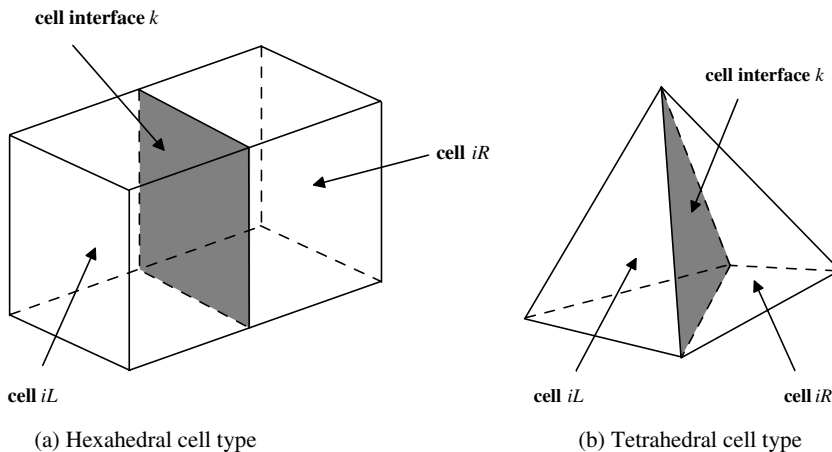
Algorithm 1. Procedures of locating breakdown regions and Boundary-I

Subroutine *Set_Breakdown_domain_Boundary-I*

```

Input both of the right- and the left-hand side cells for each cell interface.
Input  $P_{Tne}$  and  $Kn_{max}$  of each cell from the last iterative solution.
#  $D_j$ : identifier of the domain types for the specific cell  $j$ .
#  $D_j = 0$ , for the breakdown domain  $\bar{\Omega}_A$ ;  $=1$ , for the overlapping region  $\bar{\Omega}_B$ ;
#  $D_j = 2$ , for the overlapping region  $\bar{\Omega}_C$ ;  $=3$ , for the rest of the region  $\bar{\Omega}_D$ .
# Initialize array domain type number.
Set  $D = 3$  for all cells.
# Initialize array IBIF (Indicator of Boundary-I faces).
# Indicator of Boundary-I faces array records if the specific cell interface  $k$  belongs to
# one of the Boundary-I faces.
Set IBIF = 0 for each cell interface.
# Mark the cells of the breakdown domain  $\bar{\Omega}_A$  as 0.
for each cell  $i$  do
  if  $((P_{Tne})_i \geq P_{Tne}^{Thr.}$  OR  $(Kn_{max})_i \geq Kn_{max}^{Thr.})$  then
    Set  $D_i = 0$ 
  end if
end for
# Mark the faces of Boundary-I.
for each cell interface  $k$  do
   $iR$  = the right-side cell of cell interface  $k$ 
   $iL$  = the left-side cell of cell interface  $k$ 
  if  $(D_{iR} \neq D_{iL})$  then
     $IBIF_k = 1$ 
  end if
end for

```



The right-side cell iR and left-side cells iL for the specific cell interface k

Algorithm 2. Procedures of generating overlapping regions and locating Boundary-IIISubroutine *Set_overlapping_regions_and_Boundary*

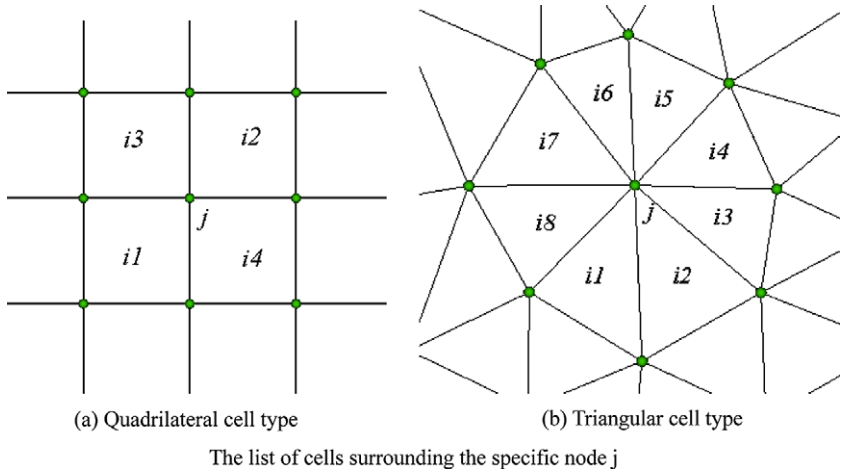
```

    Input the list of cells surrounding each node.
#   Initialize array IBIN (Indicator of Boundary-I nodes)
#   ICLN (Indicator of current layer nodes)
#   INLN (Indicator of next layer nodes)
#   Array of Indicator of Boundary-I nodes records if the specific node  $j$  belongs to one of
#   the Boundary-III faces.
#   Current layer nodes is a special node group which forms a close layer of the current
#   extended overlapping regions and breakdown domains in each extension of
#   overlapping regions layer-by-layer. Once each layer extension of overlapping is
#   completed, nodes of Current layer will be updated with the next layer nodes.
    Set IBIN = 0, ICLN = 0 and INLN = 0 for each node.
#   Indicator of Boundary-III faces array records if the specific cell interface  $k$  belongs to
#   one of the Boundary-III faces.
#   Initialize array IBIIIF (Recorder of Boundary-III faces)
    Set IBIIIF = 0 for each cell interface.
#   Preset the numbers of cell layers for each overlapping domain  $\bar{\Omega}_B$  and  $\bar{\Omega}_C$ .
    Set No_layers(1) = 4
    Set No_layers(2) = 2
#   Mark the nodes on Boundary-I
    for each cell interface  $k$  such that IBIF $_k$  == 1 do
        for each node  $j$  of cell interface  $k$  do
            IBIN $_j$  = 1
        end for
    end for
#   Nodes on the on Boundary-I is the first close node layer of the breakdown domains.
#   Mark all the nodes on Boundary-I as the nodes of currently searched node layer.
    ICLN(:) = IBIN(:)
#   Mark cells of domain  $\bar{\Omega}_B(R = 1)$  and  $\bar{\Omega}_C(R = 2)$  by searching layer-by-layer
#   extension.
    for overlapping region  $R = 1, 2$  do
        Set  $n = 1$ 
        while ( $n \leq$  No_layers( $R$ )) do
            for each node  $j$  such that ICLN $_j$  == 1 do
                for each cell  $i$  surrounding node  $j$  such that  $D_i$  == 3 do
                    Set  $D_i = R$ 
                    for each node  $k$  of cell  $i$  such that ICLN $_k$  == 0 do
                        if (INLN $_k$  == 0) then
                            INLN $_k$  == 1
                        end if
                    end for
                end for
            end for
            ICLN(:) = INLN(:)
            INLN = 0
             $n = n + 1$ 
        end while
    end for
#   Mark the faces of Boundary-III
    FBIII = 0

```

```

# Remark:  $D_i = 3$  means the cell  $i$  belong to  $\overline{\Omega}_D$  in NS domain
for each cell interface  $k$  do
   $iR$  = the right-side cell of cell interface  $k$ 
   $iL$  = the left-side cell of cell interface  $k$ 
  if ( $(D_{iR} == 3$  AND  $D_{iL} == 2)$  OR  $(D_{iR} == 2$  AND  $D_{iL} == 3)$ ) then
     $FBIII_k = 1$ 
  end if
end for
    
```



Algorithm 3. General procedures of the proposed coupled DSMC–NS method
Main loop

```

Set MCI = maximum number of coupling iterations
# Initial “one-shot” HYB3D for whole domain
call NS solver HYB3D (for the whole simulation domain)
# Coupling Iterations
   $loop = 1$ 
  while ( $loop \leq MCI$ ) do
    call Subroutine Set_breakdown_domai_and_Boundary-I
    call Subroutine Set_overlapping_regions_and_Boundary-III
    call Subroutine Extract_Boundary-III_data_for_DSMC_solver
# For domain  $\overline{\Omega}_A \cup \overline{\Omega}_B \cup \overline{\Omega}_C$ 
    call DSMC code PDSC
    call Subroutine Extract_Boundary-I_data_for_NS_solver
# For domain  $\overline{\Omega}_B \cup \overline{\Omega}_C \cup \overline{\Omega}_D$ 
    call NS solver HYB3D
    call Subroutine Solution_update
     $loop = loop + 1$ 
  end do
    
```

Algorithm 4. Procedures of extracting Boundary-III data for DSMC solver
 Subroutine *Extract_Boundary-III_data_for_DSMC_solver*

```

 $n = 0$ 
for each cell interface  $k$  such that  $FBIII_k = 1$  do
    
```

```

n = n + 1
iR = the right-hand side cell of cell interface k
iL = the left-hand side cell of cell interface k
average flow properties of both cell iR and iL as flow data of the n-th face of DSMC hybrid boundary
end for

```

Algorithm 5. Procedures of extracting Boundary-I data for NS solver

Subroutine *Extract_Boundary-I_data_for_NS_solver*

```

for each cell interface k such that  $FBI_k = 1$  do
  iR = the right-hand side cell of cell interface k
  iL = the left-hand side cell of cell interface k
  if ( $D_{iR} = 0$ ) then
    set flow data of cell interface k with flow properties of cell iR from DSMC domain
  else
    set flow data of cell interface k with flow properties of cell iL from DSMC domain
  end if
end for

```

Acknowledgments

This work was performed under NCC3-994 for the National Aeronautics and Space Administration (NASA) Constellation University Institutes Project (CUIP) program in USA. Financial support for the first author by National Science Council (NSC91-2212-E-009-045) and National Space Program office (92-NSPO(A)-PC-FA06-01) of Taiwan is also highly appreciated. We thank for the parallel computing resource provided by National Center for High-performance Computing (NCHC) of Taiwan. Finally, Dr. Y.-S. Chen at NSPO of Taiwan is also highly appreciated for several useful discussions during the study.

References

- [1] M. Taniguchi, H. Mori, R. Nishihira, T. Niimi, Experimental analyses of flow field structures around clustered linear aerospikes nozzles, in: M. Capitelli (Ed.), 24th International Symposium on Rarefied Gas Dynamics, Bari, Italy, July 10–16, 2004.
- [2] M.S. Ivanov, D.V. Khotyanovsky, A.N. Kudryavtsev, P.V. Vashchenkov, G.N. Markelov, A.A. Schmidt, Numerical study of backflow for nozzle plumes expanding into vacuum, in: 37th AIAA Thermophysics Conference, AIAA Paper 2004-2687, 2004.
- [3] G.A. Bird, *Molecular Gas Dynamics and the Direct Simulation of Gas Flows*, Oxford University Press, New York, 1994.
- [4] O. Aktas, N.R. Aluru, A combined continuum/DSMC technique for multiscale analysis of microfluidic filters, *J. Comput. Phys.* 178 (2002) 342, doi:10.1006/jcph.2002.7030.
- [5] A.L. Garcia, J.B. Bell, W.Y. Crutchfield, B.J. Alder, Adaptive mesh and algorithm refinement using direct simulation Monte Carlo, *J. Comput. Phys.* 154 (1999) 134.
- [6] C.E. Glass, P.A. Gnoffo, A 3-D coupled CFD–DSMC solution method with application to the mars sample return orbiter, NASA Report TM-2000-210322, 2000. Available from: <<http://techreports.larc.nasa.gov/ltrs/PDF/2000/tm/NASA-2000-tm210322.pdf>>.
- [7] W.-L. Wang, Q.-H. Sun, I.D. Boyd, Towards development of a hybrid DSMC–CFD method for simulating hypersonic interacting flows, in: 8th AIAA/ASME Joint Thermophysics and Heat Transfer Conference, AIAA Paper 2002-3099, 2002.
- [8] R. Roveda, D.B. Goldstein, P.L. Varghese, Hybrid Euler/particle approach for continuum/rarefied flows, *J. Spacecraft Rockets* 35 (1998) 258.
- [9] J.-S. Wu, K.-C. Tseng, Parallel DSMC method using dynamic domain decomposition, *Int. J. Numer. Meth. Eng.* 63 (2005) 37.
- [10] J.-S. Wu, Y.-Y. Lian, Parallel three-dimensional direct simulation Monte Carlo method and its applications, *Comp. Fluids* 32 (2003) 1133.
- [11] J.-S. Wu, K.-C. Tseng, F.-Y. Wu, Parallel three dimensional direct simulation Monte Carlo method using unstructured adaptive mesh and variable time step, *Comp. Phys. Commun.* 162 (2004) 166.
- [12] J.-S. Wu, K.-C. Tseng, U.-M. Lee, Y.-Y. Lian, Development of a general parallel three-dimensional direct simulation Monte Carlo code, in: M. Capitelli (Ed.), 24th International Symposium on Rarefied Gas Dynamics, Bari, Italy, July 10–16, 2004.

- [13] R.P. Koomullil, B.K. Soni, C.-T. Huang, Navier–Stokes simulation on hybrid grids, in: 34th Aerospace Sciences Meeting and Exhibit, AIAA 96-0768, 1996.
- [14] R.P. Koomullil, B.K. Soni, C.-T. Huang, Unsteady flow simulations on hybrid grids, in: L. Sakell, D.D. Knight, Proceedings of 1st AFOSR Conference in Dynamic Motion CFD, Rutgers University, NJ, June 3–5, 1996, pp. 427–434.
- [15] R.P. Koomullil, B.K. Soni, C.-T. Huang, Flow simulations on generalized grids, in: B.K. Soni, J.F. Thompson, J. Hauser, P. Eiseman, Proceedings of 5th International Conference on Numerical Grid Generation in Computation Fluid Dynamics and Related Fields, Mississippi State University, MS, April 1–5, 1996, pp. 527–536.
- [16] R.P. Koomullil, B.K. Soni, Flow simulation using generalized static and dynamics grids, AIAA J. 37 (1999) 1551.
- [17] G. Karypis, V. Kumar, METIS: A Software Package for Partitioning Unstructured Graphs, Partitioning Meshes, and Computing Fill-Reducing Orderings of Sparse Matrices, 1998. Available from: <<http://www-users.cs.umn.edu/~karypis/metis>>.
- [18] G. Karypis, V. Kumar, ParMETIS 3.1: An MPI-based Parallel Library for Partitioning Unstructured Graphs, Meshes, and Computing Fill-Reducing Orderings of Sparse Matrices, 2003. Available from: <<http://www-users.cs.umn.edu/~karypis/metis/parmetis>>.
- [19] D.M. Nicol, J.H. Saltz, Dynamic remapping of parallel computations with varying resource demands, IEEE Trans. Comp. 37 (1988) 1073.
- [20] V. Venkatakrishnan, Convergence to steady state solutions of the Euler equations on unstructured grids with limiters, J. Comput. Phys. 118 (1995) 120.
- [21] W.-L. Wang, I.D. Boyd, Predicting continuum breakdown in hypersonic viscous flows, Phys. Fluids 15 (2003) 91.
- [22] C. Borgnakke, P.S. Larsen, Statistical collision model for Monte Carlo simulation of polyatomic gas mixture, J. Comput. Phys. 18 (1975) 405.
- [23] R.P. Koomullil, Flow Simulation System for Generalized Static and Dynamics Grids, Ph.D. Dissertation, Mississippi State University, 1997.
- [24] R.P. Koomullil, D.S. Thompson, B.K. Soni, Iced airfoil simulation using generalized grids, J. Appl. Numer. Math. 46 (2003) 319.
- [25] T.J. Barth, D.C. Jespersen, The Design and Application of Upwind Schemes on Unstructured Meshes, AIAA Paper 89-0366, 1989.
- [26] V. Venkatakrishnan, On the Accuracy of Limiters and Convergence to Steady State Solutions, AIAA Paper 93-0880, 1993.
- [27] A. Garcia, B. Alder, Generation of the Chapmann–Enskog distribution, J. Comput. Phys. 140 (1998) 66.
- [28] T. Soga, M. Takanishi, M. Yasuhara, Experimental study of interaction of underexpanded jets, in: H. Oguchi (Ed.), 14th International Symposium on Rarefied Gas Dynamics, Tsukuba Science City, Japan, 1984, pp. 485–493.